ETSI GR RIS 003 V1.1.1 (2023-06)

GROUP REPORT

Reconfigurable Intelligent Surfaces (RIS); Communication Models, Channel Models, Channel Estimation and Evaluation Methodology

ETSI

650 Route des Lucioles
F-06921 Sophia Antipolis Cedex - FRANCE

Tel.: +33 4 92 94 42 00   Fax: +33 4 93 65 47 16

Siret N° 348 623 562 00017 - APE 7112B
Association à but non lucratif enregistrée à la
Sous-Préfecture de Grasse (06) N° w061004871

Important notice

The present document can be downloaded from:
https://www.etsi.org/standards-search

The present document may be made available in electronic versions and/or in print. The content of any electronic and/or print versions of the present document shall not be modified without the prior written authorization of ETSI. In case of any existing or perceived difference in contents between such versions and/or in print, the prevailing version of an ETSI deliverable is the one made publicly available in PDF format at www.etsi.org/deliver.

Users of the present document should be aware that the document may be subject to revision or change of status. Information on the current status of this and other ETSI documents is available at
https://portal.etsi.org/TB/ETSIDeliverableStatus.aspx

If you find errors in the present document, please send your comment to one of the following services:
https://portal.etsi.org/People/CommiteeSupportStaff.aspx

If you find a security vulnerability in the present document, please report it through our
Coordinated Vulnerability Disclosure Program:
https://www.etsi.org/standards/coordinated-vulnerability-disclosure

Notice of disclaimer & limitation of liability

The information provided in the present deliverable is directed solely to professionals who have the appropriate degree of experience to understand and interpret its content in accordance with generally accepted engineering or other professional standard and applicable regulations.
No recommendation as to products and services or vendors is made or should be implied.
No representation or warranty is made that this deliverable is technically accurate or sufficient or conforms to any law and/or governmental rule and/or regulation and further, no representation or warranty is made of merchantability or fitness for any particular purpose or against infringement of intellectual property rights.
In no event shall ETSI be held liable for loss of profits or any other incidental or consequential damages.

Any software contained in this deliverable is provided "AS IS" with no warranties, express or implied, including but not limited to, the warranties of merchantability, fitness for a particular purpose and non-infringement of intellectual property rights and ETSI shall not be held liable in any event for any damages whatsoever (including, without limitation, damages for loss of profits, business interruption, loss of information, or any other pecuniary loss) arising out of or related to the use of or inability to use the software.

Contents

Intellectual Property Rights

Essential patents

IPRs essential or potentially essential to normative deliverables may have been declared to ETSI. The declarations pertaining to these essential IPRs, if any, are publicly available for **ETSI members and non-members**, and can be found in ETSI SR 000 314: *"Intellectual Property Rights (IPRs); Essential, or potentially Essential, IPRs notified to ETSI in respect of ETSI standards"*, which is available from the ETSI Secretariat. Latest updates are available on the ETSI Web server (https://ipr.etsi.org/).

Pursuant to the ETSI Directives including the ETSI IPR Policy, no investigation regarding the essentiality of IPRs, including IPR searches, has been carried out by ETSI. No guarantee can be given as to the existence of other IPRs not referenced in ETSI SR 000 314 (or the updates on the ETSI Web server) which are, or may be, or may become, essential to the present document.

Trademarks

The present document may include trademarks and/or tradenames which are asserted and/or registered by their owners. ETSI claims no ownership of these except for any which are indicated as being the property of ETSI, and conveys no right to use or reproduce any trademark and/or tradename. Mention of those trademarks in the present document does not constitute an endorsement by ETSI of products, services or organizations associated with those trademarks.

DECT™, **PLUGTESTS™**, **UMTS™** and the ETSI logo are trademarks of ETSI registered for the benefit of its Members. **3GPP™** and **LTE™** are trademarks of ETSI registered for the benefit of its Members and of the 3GPP Organizational Partners. **oneM2M™** logo is a trademark of ETSI registered for the benefit of its Members and of the oneM2M Partners. **GSM**® and the GSM logo are trademarks registered and owned by the GSM Association.

Foreword

This Group Report (GR) has been produced by ETSI Industry Specification Group (ISG) Reconfigurable Intelligent Surfaces (RIS).

Modal verbs terminology

In the present document "**should**", "**should not**", "**may**", "**need not**", "**will**", "**will not**", "**can**" and "**cannot**" are to be interpreted as described in clause 3.2 of the ETSI Drafting Rules (Verbal forms for the expression of provisions).

"**must**" and "**must not**" are **NOT** allowed in ETSI deliverables except when used in direct citation.

1 Scope

The present document is intended to study:

a) communication models that strike a suitable trade-off between electromagnetic accuracy and simplicity for performance evaluation and optimization at different frequency bands;

b) channel models (deterministic and statistical) that include path-loss and multipath propagation effects, as well as the impact of interference for application to different frequency bands;

c) channel estimation, including reference scenarios, estimation methods, and system designs; and

d) key performance indicators and the methodology for evaluating the performance of RIS for application to wireless communications, including the coexistence between different network operators, and for fairly comparing different transmission techniques, communication protocols, and network deployments.

2 References

2.1 Normative references

Normative references are not applicable in the present document.

2.2 Informative references

References are either specific (identified by date of publication and/or edition number or version number) or non-specific. For specific references, only the cited version applies. For non-specific references, the latest version of the referenced document (including any amendments) applies.

NOTE: While any hyperlinks included in this clause were valid at the time of publication, ETSI cannot guarantee their long term validity.

The following referenced documents are not necessary for the application of the present document but they assist the user with regard to a particular subject area.

[i.1] ETSI GR RIS 001 (V1.1.1): "Reconfigurable Intelligent Surfaces (RIS); Use Cases, Deployment Scenarios and Requirements".

[i.2] ETSI TR 138 901 (V16.1.0): "5G; Study on channel model for frequencies from 0.5 to 100 GHz (3GPP TR 38.901 version 16.1.0 Release 16)".

[i.3] Recommendation ITU-R SM.329: "Unwanted emissions in the spurious domain".

[i.4] M. Di Renzo, F. H. Danufane and S. Tretyakov: "Communication Models for Reconfigurable Intelligent Surfaces: From Surface Electromagnetics to Wireless Networks Optimization", in Proceedings of the IEEE[TM], 2022, doi: 10.1109/JPROC.2022.3195536.

[i.5] G. Gradoni and M. Di Renzo: "End-to-End Mutual Coupling Aware Communication Model for Reconfigurable Intelligent Surfaces: An Electromagnetic-Compliant Approach Based on Mutual Impedances", in IEEE[TM] Wireless Communications Letters, vol. 10, no. 5, pp. 938-942, May 2021, doi: 10.1109/LWC.2021.3050826.

[i.6] W. Tang et al.: "Wireless communications with reconfigurable intelligent surface: Path loss modeling and experimental measurement", IEEE[TM] Trans. Wireless Commun., vol. 20, no. 1, pp. 421-439, January 2021.

[i.7] W. Tang et al.: "Path loss modeling and measurements for reconfigurable intelligent surfaces in the millimeter-wave frequency band", IEEE[TM] Transactions on Communications 70, no. 9 (2022): 6259-6276.

[i.8]   S. W. Ellingson: "Path loss in reconfigurable intelligent surface-enabled channels", 2021 IEEE[TM] 32nd Annual International Symposium on Personal, Indoor and Mobile Radio Communications (PIMRC).

[i.9]   F. H. Danufane et al.: "On the Path-Loss of Reconfigurable Intelligent Surfaces: An Approach Based on Green's Theorem Applied to Vector Fields," in IEEE[TM] Transactions on Communications, vol. 69, no. 8, pp. 5573-5592, August 2021.

[i.10]   Emil Björnson and Luca Sanguinetti: "Rayleigh fading modeling and channel hardening for reconfigurable intelligent surfaces", IEEE[TM] Wireless Communications Letters 10, no. 4 (2020): 830-834.

[i.11]   N. S. Perović et al.: "Achievable Rate Optimization for MIMO Systems With Reconfigurable Intelligent Surfaces", in IEEE[TM] Transactions on Wireless Communications, vol. 20, no. 6, pp. 3865-3882, June 2021.

[i.12]   A. Abrardo et al.: "MIMO Interference Channels Assisted by Reconfigurable Intelligent Surfaces: Mutual Coupling Aware Sum-Rate Optimization Based on a Mutual Impedance Channel Model", in IEEE[TM] Wireless Communications Letters, vol. 10, no. 12, pp. 2624-2628, December 2021.

[i.13]   Ibrahim Yildirim and Ertugrul Basar: "Channel Modeling in RIS‐Empowered Wireless Communications", in Intelligent Reconfigurable Surfaces (IRS) for Prospective 6G Wireless Networks, IEEE[TM], 2023, pp.123-148, doi: 10.1002/9781119875284.ch7.

[i.14]   A. Saleh and R. Valenzuela: "A statistical model for indoor multipath propagation", in IEEE[TM] Journal of Selected Areas in Communications, vol. 5, no. 2, pp. 128-137, February 1987.

[i.15]   C. Pan et al.: "An Overview of Signal Processing Techniques for RIS/IRS-Aided Wireless Systems", in IEEE[TM] Journal of Selected Topics in Signal Processing, vol. 16, no. 5, pp. 883-917, August 2022.

[i.16]   A. Díaz-Rubio and S. A. Tretyakov: "Macroscopic Modeling of Anomalously Reflecting Metasurfaces: Angular Response and Far-Field Scattering", in IEEE[TM] Transactions on Antennas and Propagation, vol. 69, no. 10, pp. 6560-6571, October 2021.

[i.17]   V. Degli-Esposti et al.: "Reradiation and Scattering from a Reconfigurable Intelligent Surface: A General Macroscopic Model", in IEEE[TM] Transactions on Antennas and Propagation, 2022.

[i.18]   B. Sihlbom, et al.: "Reconfigurable Intelligent Surfaces: Performance Assessment Through a System-Level Simulator", in IEEE[TM] Wireless Communications, 2022.

[i.19]   3GPP TR 37.885: "Study on evaluation methodology of new Vehicle-to-Everything (V2X) use cases for LTE and NR".

[i.20]   ETSI TR 137 910: "5G; Study on self evaluation towards IMT-2020 submission (3GPP TR 37.910)".

3   Definition of terms, symbols and abbreviations

3.1   Terms

For the purposes of the present document, the terms given in ETSI GR RIS 001 [i.1] apply.

3.2   Symbols

Void.

3.3 Abbreviations

For the purposes of the present document, the following abbreviations apply:

2D	2 Dimensional
3D	3 Dimensional
AoA	Angle of Arrival
AoD	Angle of Departure
AWGN	Additive White Gaussian Noise
BLER	Block Error Rate
BS	Base Station
CDL	Clustered Delay Line
CDS	Coherent Demodulation Scheme
CSI	Channel State Information
DFT	Discrete Fourier Transform
DFT-S	Discrete Fourier Transform Spread
DL	Downlink
DMRS	Demodulation Reference Signal
DoA	Direction of Arrival
EIRP	Effective Isotropic Radiated Power
EM	Electromagnetic
EMC	Electromagnetic Compatibility
EMF	Electromagnetic Field
gNB	g Node B
HARQ	Hybrid Automatic Repeat Request
HITRAN	High resolution Transmission
HMIMOS	Holographic Multiple Input Multiple Output Surface
LLS	Link-Level Simulator
LOS	Line Of Sight
LS	Least Square
MAC	Medium Access Control
MCL	Minimum Coupling Loss
MCS	Modulation and Coding Scheme
MIL	Hardware link budget
MIMO	Multiple-Input Multiple-Output
MISO	Multiple-Input Single-Output
MPL	Mechanically Pumped fluid Loop
MU	Multi User
NB	Node B
NCDS	Non Coherent Demodulation Scheme
NLOS	Non Line Of Sight
NR	New Radio
nRB	number of Resource Block
nSC	number of Sub-Carriers per resource block
NW	Network
O2I	Outdoor-to-Indoor
O2O	Outdoor-to-Outdoor
OFDM	Orthogonal Frequency-Division Multiplexing
PDSCH	Physical Downlink Shared Channel
PHY	Physical layer
PUSCH	Physical Uplink Shared Channel
RB	Resource Block
RF	Radio Frequency
RIS	Reconfigurable Intelligent Surfaces
RSE	Radiated Spurious Emission
RTT	Round-Trip Time
RX	Receiver
SAR	Specific Absorption Rate
SDU	Service Data Unit
SIMO	Single-Input Multiple-Output
SINR	Signal-to-Interference-Noise Ratio

SISO	Single-Input Single-Output
SM	Spatial Modulation
SNR	Signal-to-Noise Ratio
SV	Saleh-Valenzuela
TBA	To Be Added
TdoA	Time difference of Arrival
ToA	Time of Arrival
TRP	Total Radiated Power
TRxP	Transmission and Reception Point
TxRU	Transmit Radio Unit
UE	User Equipment
UL	Uplink
ULA	Uniform Linear Array
UMa	Urban Macro
UMi	Urban Micro
US	United States
WB	Wide-Band

4   Introduction

4.1   General Description

In this clause, the definition of RIS and relevant scenarios are described.

NOTE: The descriptions provided in the present document are aligned with those in ETSI GR RIS 001 [i.1].

4.2   Definition of RIS

Broadly an RIS is defined as follows:

- It is a surface, i.e. it is not a volumetric material, in order to reduce the implementation complexity, the losses, etc. while still being able to fully control the electromagnetic waves.

- It is an engineered (or intelligent) surface, i.e. it can realize functions that a non-engineered surface (i.e. a metal plate) cannot realize.

- It is reconfigurable, i.e. its response can be adapted over time based on the network conditions. The reconfigurability encompasses multiple functions including controlled reflection, refraction, scattering, modulation, etc.

4.3   Types of RIS

An RIS can be defined in terms of the single or multiple functions that it can realize:

- **Reflecting surfaces:** This is an RIS that is capable of modifying the angle of reflection of an incident wave.

- **Refracting surfaces:** This is an RIS that is capable of modifying the angle of refraction (transmission) of an incident wave.

- **Joint reflecting and refracting surfaces:** This is an RIS that is capable of simultaneously modifying the angle of reflection and refraction of an incident wave.

- **Transmitting or information surfaces:** This is an RIS that is capable of encoding data and to realize single-RF (single-stream or multi-stream) transmitters. Examples include RIS that encode data onto the activations patterns of the unit cells or the synthetized radiation patterns.

- **Surface for ambient backscattering:** This is an RIS that can simultaneously reflect or refract the incident waves and simultaneously modulate data onto the reflected or refracted wave.

- **Surfaced for tuned randomness:** This is an RIS that is configured in order to increase the scattering in a given area.

- **Absorbing surfaces:** This is an RIS that is configured to minimize the scattered field.

- **Communication and sensing surfaces:** This is an RIS with integrated communication and sensing capabilities, i.e. a surface that can simultaneously reflect a wave and detect the presence of objects.

4.4   Deployment scenarios

RIS can be utilized in different scenarios, including the following.

Enhanced connectivity and reliability

- Connectivity and reliability boosted by a single RIS.

- Connectivity and reliability boosted by individually controlled multiple RIS.

- Connectivity and reliability enabled by multiple RIS.

- Connectivity and reliability boosted by a single multitenant RIS.

- RIS-aided mobile edge computing.

Enhanced localization and sensing

- Unambiguous localization under favourable problem geometry with a minimal number of base stations.

- Non Line Of Sight (LOS) mitigation for better service coverage and continuity in far-field conditions.

- Non LOS mitigation for better service coverage and continuity in near-field conditions.

- On-demand multi-user and multi-accuracy service provision.

- Opportunistic detection/sensing of passive objects through multi-link radio activity monitoring.

- RIS-assisted search-and-rescue operations in emergency scenarios.

- Localization without BSs using a single or multiple RIS.

- RIS-aided radio environment mapping for fingerprinting localization.

- Radar localization/detection of passive target(s) with hybrid RIS.

Enhanced sustainability and security

- Deployments of RIS to increase the energy efficiency and reduce the power consumption.

- Deployments of RIS to increase security.

5   Models for RIS

5.1   Models for communications

5.1.1   General description

Three main communication models for RIS can be adopted [i.4]:

- Locally periodic discrete model.

- Mutually-coupled antenna model.

- Inhomogeneous sheets of surface impedance model.

5.1.2   Locally periodic discrete model

A widely used model for RIS is based on a locally periodic design, in which periodic boundary conditions are applied at the unit cell level. Accordingly, each RIS reconfigurable element is associated with a set of complex-valued coefficients (the RIS alphabet). Each element of the alphabet is obtained by appropriately configuring the electronic circuits of the RIS reconfigurable element. For ease of description, it is assumed that the RIS operates as a reflecting surface. From the physical standpoint, therefore, the complex-valued coefficient has the meaning of a reflection coefficient, i.e. the ratio between the reflected electric field and the incident electric field, of an infinite RIS whose elements are all configured to the same state. Therefore, the corresponding equivalent structure is a homogeneous surface that realizes specular reflection. According to this definition, each RIS reconfigurable element is characterized by means of locally periodic boundary conditions, and, since an RIS is not endowed with power amplifiers, the reflection coefficients have an amplitude that is, by definition, less than one. However, this neither necessarily implies that the amplitude is a constant independent of the phase nor that the amplitude and the phase can be optimized independently of one another.

5.1.3   Mutually-coupled antenna model

To account for the mutual coupling among closely-spaced RIS elements, a model based on loaded RIS elements illustrated in Figure 1 can be used.
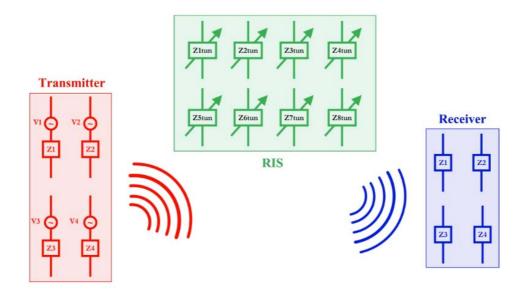

Figure 1: Mutually coupled antenna model

The model resembles a conventional single transmitter-receiver pair Multiple-Input Multiple-Output (MIMO) communication link in the presence of an RIS. The transmitter and the receiver are equipped with multiple-antenna elements. For ease of representation, the antenna elements are assumed to be thin wire dipoles. The model can be utilized for application to radiating elements different from thin wire dipoles. Each antenna element at the transmitter is driven by a voltage generator that models the transmit feed line, and each antenna element at the receiver is connected to a load impedance that mimics the receive electronic circuit. The transmission between the transmitter and the receiver is assisted by an RIS, which comprises several scattering elements that are independently configurable (by an external controller) through tuneable impedances. The end-to-end transfer function that accounts for the scattering from the RIS can be formulated as follows [i.5]:

$$\mathbf{H} = (\mathbf{I}_{L0} + \boldsymbol{\psi}_{r,r}\mathbf{Z}_r^{-1} - \boldsymbol{\psi}_{r,t}(\boldsymbol{\psi}_{t,t} + \mathbf{Z}_t)^{-1}\boldsymbol{\psi}_{t,r}\mathbf{Z}_r^{-1})^{-1}\boldsymbol{\psi}_{r,t}(\boldsymbol{\psi}_{t,t} + \mathbf{Z}_t)^{-1}$$

where:

$$\boldsymbol{\psi}_{t,t} = \mathbf{Z}_{t,t} - \mathbf{Z}_{t,s}(\mathbf{Z}_{s,s} + \mathbf{Z}_{\text{tun}})^{-1}\mathbf{Z}_{s,t}$$

$$\boldsymbol{\psi}_{t,r} = \mathbf{Z}_{t,r} - \mathbf{Z}_{t,s}(\mathbf{Z}_{s,s} + \mathbf{Z}_{\text{tun}})^{-1}\mathbf{Z}_{s,r}$$

$$\boldsymbol{\psi}_{r,t} = \mathbf{Z}_{r,t} - \mathbf{Z}_{r,s}(\mathbf{Z}_{s,s} + \mathbf{Z}_{\text{tun}})^{-1}\mathbf{Z}_{s,t}$$

$$\boldsymbol{\psi}_{r,r} = \mathbf{Z}_{r,r} - \mathbf{Z}_{r,s}(\mathbf{Z}_{s,s} + \mathbf{Z}_{\text{tun}})^{-1}\mathbf{Z}_{s,r}$$

Each term of the equations can be computed either numerically or in closed-form [i.5]. The proposed model is conveniently formulated in a MIMO-like form, which enables one to use optimization methods for optimizing the tenable loads connected to each scattering element.

In the far-field of each scattering element of the transmitter, receiver, and RIS, the following simplified model can be used [i.5]:

$$\mathbf{H}_{r,t} \approx (\mathbf{I}_{L0} + \mathbf{Z}_{r,r}\mathbf{Z}_r^{-1})^{-1}(\mathbf{Z}_{t,t} + \mathbf{Z}_t)^{-1}(\mathbf{Z}_{r,t} - \mathbf{Z}_{r,s}(\mathbf{Z}_{s,s} + \mathbf{Z}_{\text{tun}})^{-1}\mathbf{Z}_{s,t})$$

This simplified model has wide applicability in wireless communications because it is expected to operate in the far-field of each scattering element, but not in the far-field of the entire surface.

5.1.4   Inhomogeneous sheets of surface impedance

More precisely, an RIS whose unit cells have sizes and inter-distances much smaller than the wavelength is homogenizable and can be modeled as a continuous surface sheet through appropriate surface functions, i.e. surface impedances. This modeling approach is not dissimilar from the characterization of bulk (three-dimensional) metamaterials, which are usually represented through effective permittivity and permeability functions that determine the wave phenomena based on Maxwell's equations. The only difference is that a metasurface is better modeled by effective surface parameters, which manifest themselves in electromagnetic problems that are formulated as effective boundary conditions. These boundary conditions can be expressed in terms of surface polarizabilities, surface susceptibilities, or surface impedances (or admittances). Under these assumptions, an RIS can be modeled as an inhomogeneous sheet of polarizable particles (the unit cells) that is characterized by an electric surface impedance and a magnetic surface admittance, which, for general wave transformations, are dyadic tensors. These two dyadic tensors constitute the macroscopic homogenized model of an RIS. Once the homogenized and continuous electric surface impedance and magnetic surface admittance are obtained based on the desired wave transformations, the microscopic structure and physical implementation of the RIS in terms of unit cells are obtained. Generally speaking, once the macroscopic surface impedance and admittance are determined, appropriate geometric arrangements of sub-wavelength unit cells and the associated tuning circuits that exhibit the corresponding electric and magnetic response are characterized by, typically, using full-wave electromagnetic simulations.

5.2   Models for radio localization and sensing

5.2.1   Scenarios

5.2.1.1   Localization scenarios

With cellular localization, the User Equipment (UE) location can be estimated based on a variety of measurements from the received signal, including the signal strength, Time of Arrival (ToA), Round-Trip Time (RTT), Angle of Arrival (AoA) and Angle of Departure (AoD). The scenarios can be categorized as SISO localization, MISO localization, SIMO localization, and MIMO localization as shown in Figure 2, where the symbols τ, ϕ, and θ indicate ToAs, AoDs, and AoAs, respectively.

Figure 2: Localization scenarios

5.2.1.2   SISO localization

In this scenario, the Base Station (BS) and UE are both equipped with a single antenna.

In the SISO system with 1 RIS and 1 BS, Wide-Band (WB) pilots should be used to measure the ToAs for the direct (i.e. the path BS-UE) and the reflected (i.e. the path BS-RIS-UE) paths, from which the resulting TdoA can be can calculated and so the corresponding hyperboloid in 3D space. By using different RIS phase profiles at different transmission times, the AoD from the RIS to the UE can be estimated, which geometrically translates to a half-line. Therefore, the UE position can be calculated via the intersection between such half-line and the abovementioned hyperboloid.

In the SISO system with 2 (more than 1) RIS and 1 BS, UE positioning even with NB signalling can be performed, which does not allow ToA estimation. Indeed, the UE position can be estimated via the intersection of the two half-lines corresponding to the AoDs from the RIS. The direct BS-UE path does not carry any position information, thus localization can be performed even when the direct path is blocked.

In the SISO system with 1 RIS in the absence of a BS, the RTT and the AoD from the RIS to the UE can be measured. Geometrically, they respectively correspond to a sphere centered in the RIS and a half-line originated in the RIS, whose intersection returns the UE position estimate.

5.2.1.3   MISO localization

In this scenario, the BS is equipped with multiple antennas while the UE is with a single antenna. The UE position can be estimated by intersecting the two half-lines corresponding to the two AoDs from the BS and the RIS.

5.2.1.4   SIMO localization

In this scenario, the UE is equipped with multiple antennas while the BS is with a single antenna. Two AoAs and one AoD from the RIS can be measured. Using the two AoAs, the user on (part of) a spindle Torus can be located, whose intersection with the line corresponding the AoD locates the UE. Then the UE orientation can be estimated via the two AoAs.

5.2.1.5   MIMO localization

In this scenario, both the BS and the UE are equipped with multiple antennas. The UE position can be estimated via the two AoDs (by intersecting the two corresponding half-lines) while the UE orientation can be derived from the two AoAs.

5.2.1.6   RIS-aided and RIS-standalone

In 3GPP, location (or position) can be estimated from NW (i.e. gNB, TRP, etc.) and/or UE side. For instance, timing difference based (i.e. DL/UL TdoA) and angular based (i.e. DL/UL DoA, AoA, etc.) algorithms are supported in 3GPP standards. When RIS is involved in the localization, two RIS localization scenarios can be considered:

- RIS-aided localization.

- RIS-standalone localization.

RIS-aided localization refers to the case where RIS can assist NW and UE for location estimation as shown in Figure 3 (see scenario (a)). RIS-standalone localization refers to the case where RIS and UE are majorly involved for location estimation but NW can still assist the localization without the awareness of UE as shown in Figure 3 (see scenario (b)).

Figure 3: RIS localization scenarios (a) RIS-assisted (b) RIS-standalone

Based on the RIS deployment, RIS localization can be categorized in terms of the following factors for different scenarios, i.e. RIS-aided and RIS-standalone localization:

- With or without the direct path between UE and NW.

- Operating regime: far-field or near-field.

- Frequency range: sub-6 GHz or mmWave (i.e. FR2, FR2+, etc.).

- Antenna setting between NW and UE: SISO, SIMO, MISO, and MIMO.

- RIS type: passive, semi-active, or active.

- RIS control setting: e.g. the number of RIS elements used for the localization.

There are three channel paths in the RIS-aided communication (BS-RIS-UE) which can be categorized as the BS-RIS path, the RIS-UE path, and (BS-UE) path (or direct path). Therefore, when considering RIS localization, it needs to be further analysed whether there exists a direct path (i.e. BS-UE) or not. This is because when there is a direct path, the UE localization may reuse existing position techniques or can be enhanced with RIS assistance. In addition, operating regimes such as far-field or near-field may have nominal impact factors for the accuracy of the location estimation. Also, RIS type in terms of semi-active or active RIS, the active RIS and the number of elements used for localization could have an impact for location estimation. Finally, antenna setting between NW and UE can be specified as one of the considered factors for RIS-aided localization. For the standalone RIS localization considered, wherein the direct path is either completely blocked or severely affected and hence may not be utilized for the purpose of localization.

5.2.2   Near-field

5.2.2.1   Near-field regimes

For localization purposes, sparse parametric models are often used, where the channel is represented via a few geometric components. Figure 4 illustrates a one-ray SISO system including one RIS, where both the BS and UE are in the near field of the RIS. In this case, the received signal in the downlink can be calculated as a sum of individual rays reflected from each RIS element at the UE location.

NOTE: The received signal in the downlink can be expressed as function of the UE position.

Figure 4: The near-field regimes of the RIS-enabled signal propagation with respect to the RIS
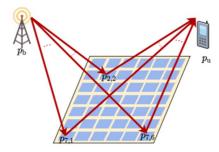
Assume there are *M* RIS while each RIS consists of *L* phase-tuneable meta-atom elements and is implemented with the single-RX-RF architecture. The user broadcasts a pilot symbol *s* with constant transmit power *P*. This symbol is received *T* times by each RIS, where during each repetition a different RIS phase profile is used. In the presence of C_m distinct channel paths, the observation during the *t*-th reception slot (*t* = 1, 2,..., *T*) at the *m*-th RIS's RX RF chain output can be mathematically expressed as follows:

$$y_{m,t} = \boldsymbol{u}_{m,t}^H \sum_{c=1}^{C_m} h_{m,c}\, \boldsymbol{\alpha}(\mathbf{p}_{m,l}, \mathbf{p}_u)s + \boldsymbol{u}_{m,t}^H \boldsymbol{w}_{m,t}$$

where $h_{m,c} = \sqrt{P_{L_{m,c}}}\, exp(j\varphi_m) \,\forall c = 1,2, \dots, C_m$ includes the gain of the *c*-th signal propagation path with parameter $P_{L_{m,c}}$ denoting the free-space pathloss. Without loss of generality, the $c = 1$ channel path represents the Line Of Sight (LOS), hence, its pathloss $P_{L_{m,1}}$ depends on the Euclidean distance $r_{m,1} = \|\mathbf{p}_m - \mathbf{p}_u\|$ with $\mathbf{p}_m$ denoting the position of *m*-th RIS; each distance $r_{m,c}$ for $c \geq 2$ is defined similarly considering the position of the corresponding scatterer. In the expression for $h_{m,c}$, $\varphi_m \sim \mathcal{U}(0, 2\pi)$ denotes a global phase offset accounting for the lack of phase synchronization between the user and the m-th RIS. The vector $\boldsymbol{u}_{m,t} \in \mathbb{C}^{L \times 1}$ is the *t*-th phase configuration of the m-th RIS. The vector $\boldsymbol{w}_{m,t} \in \mathbb{C}^{L \times 1}$ represents the Additive White Gaussian Noise (AWGN). Finally, the spatial response vector $\boldsymbol{\alpha}(\mathbf{p}_{m,l}, \mathbf{p}_u) \in \mathbb{C}^{L \times 1}$ of the user transmitted signal via multipath propagation given for *l* = 1, 2,..., *L* is as follows:

$$\left[\boldsymbol{\alpha}(\mathbf{p}_{m,l}, \mathbf{p}_u)\right]_l = exp\left(j\frac{2\pi}{\lambda}\|\mathbf{p}_{m,l} - \mathbf{p}_u\|\right)$$

with $\boldsymbol{\lambda}$ as the signal wavelength.
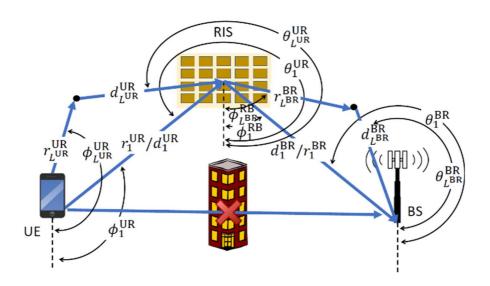
5.2.2.2   Near-field multiple paths

Figure 5: RIS localization scenario with MIMO system

Considering a Multiple-Input Multiple-Output (MIMO) system consisting of a Base Station (BS), Reconfigurable Intelligent Surfaces (RIS), and a User Equipment (UE), all the stations are equipped with Uniform Linear Arrays (ULAs) with number of antennas $N^{\mathrm{B}}, N^{\mathrm{R}}, N^{\mathrm{U}}$, respectively. As shown in Figure 5, the overall channel model $\mathbf{H} \in \mathbb{C}^{N^{\mathrm{B}} \times N^{\mathrm{U}}}$ between the BS and the UE can be modeled using a geometric model with L^{BR} and L^{UR} paths between the (BS and RIS) and (RIS and US), respectively, while assuming the Line Of Sight (LOS) between the BS and the UE to be blocked as:

$$\mathbf{H} = \mathbf{H}^{\mathrm{BR}} \mathrm{diag}(\boldsymbol{\Theta}) \mathbf{H}^{\mathrm{UR}}$$

where the diagonal matrix $\mathrm{diag}(\boldsymbol{\Theta}) \in \mathbb{C}^{N^{\mathrm{R}} \times N^{\mathrm{R}}}$ represents the phase design matrix of the RIS with diagonal $\boldsymbol{\Theta} \triangleq \left[\zeta_1 e^{j\theta_1}, \zeta_2 e^{j\theta_2}, \dots, \zeta_{N^{\mathrm{R}}} e^{j\theta_{N^{\mathrm{R}}}}\right]$, $\mathbf{H}^{\mathrm{BR}} \in \mathbb{C}^{N^{\mathrm{B}} \times N^{\mathrm{R}}}$ and $\mathbf{H}^{\mathrm{UR}} \in \mathbb{C}^{N^{\mathrm{U}} \times N^{\mathrm{R}}}$ represents the channel between the BS and the RIS the (BS and RIS) and (RIS and US), respectively. The channel between the BS and the RIS $\mathbf{H}^{\mathrm{BR}}$ can be further expressed as:

$$\mathbf{H}^{\mathrm{BR}} = \mathbf{A}(\boldsymbol{\theta}^{\mathrm{BR}}, \mathbf{d}^{\mathrm{BR}}) \mathrm{diag}(\boldsymbol{\rho}^{\mathrm{BR}}) \mathbf{A}^H(\boldsymbol{\phi}^{\mathrm{BR}}, \mathbf{r}^{\mathrm{BR}})$$

where $\mathbf{A}(\boldsymbol{\theta}^{\mathrm{BR}}, \mathbf{d}^{\mathrm{BR}}) \in \mathbb{C}^{N^{\mathrm{B}} \times L^{\mathrm{BR}}}$ and $\mathbf{A}^H(\boldsymbol{\phi}^{\mathrm{BR}}, \mathbf{r}^{\mathrm{BR}}) \in \mathbb{C}^{N^{\mathrm{R}} \times L^{\mathrm{BR}}}$ represents the steering matrices at the BS and the RIS respectively, the angles $\boldsymbol{\phi}^{\mathrm{BR}}$ and $\boldsymbol{\theta}^{\mathrm{BR}}$ are the Angle of Departure (AoD) and the Angle of Arrival (AoA), on the other hand both $\mathbf{r}^{\mathrm{BR}}$ and $\mathbf{d}^{\mathrm{BR}}$ represents the distances between the (RIS and scatterers) and (scatterers and BS), respectively. Fresnel approximation can be used to model the spherical wavefront in the near-field model. The steering matrix element corresponding to the lth path and the bth antenna element can be expressed as:

$$a_{b,l}\left(\theta_l^{\mathrm{BR}}, d_l^{\mathrm{BR}}\right) = \exp\left(j\left[b\omega_l^{\mathrm{BR}} + b^2 \gamma_l^{\mathrm{BR}}\right]\right),$$

where:

$$\omega_l^{\mathrm{BR}} \triangleq f\left(\theta_l^{\mathrm{BR}}\right) \text{ and } \gamma_l^{\mathrm{BR}} \triangleq g\left(\theta_l^{\mathrm{BR}}, d_l^{\mathrm{BR}}\right)$$

with:

$$f(\phi) = -\frac{2\pi\delta}{\lambda}\sin(\phi), \quad g(\phi, r) = \frac{\pi\delta^2}{\lambda r}\cos^2(\phi),$$

where λ is the wavelength, δ is the distance of adjacent elements in the ULA. For the diagonal matrix $\mathrm{diag}(\boldsymbol{\rho}^{\mathrm{BR}}) \in \mathbb{C}^{L^{\mathrm{BR}} \times L^{\mathrm{BR}}}$, it represents the propagation gains of each path between the RIS and BS. The propagation gain of the lth path can be modeled as:

$$\rho_l^{\mathrm{BR}} = \left(\frac{c}{4\pi(r_l^{\mathrm{BR}} + d_l^{\mathrm{BR}})f_c}\right)^{\frac{\mu}{2}} F,$$

where c is the speed of light, f_c is the carrier frequency, and F is a standard complex Gaussian random variable representing the fading. The channel $\mathbf{H}^{UR}$ can be expressed in a similar way.

5.2.2.3   Near-field single-path

In this model, a localization scenario where a gNB, equipped with an antenna array with center located in position $p_B = [x_B, y_B, z_B]^T$, performs the position and orientation estimation of a UE with center in $p_M = [x_M, y_M, z_M]^T$ and with a rotation of $\phi_M = [\alpha_M, \beta_M, \gamma_M]^T$ is considered. The geometry is reported in Figure 6. The localization is aided by the presence of a RIS, with center located at a known position $p_R = [x_R, y_R, z_R]^T$, considered as a passive reflector that supports the gNB also for communicating with the UE.
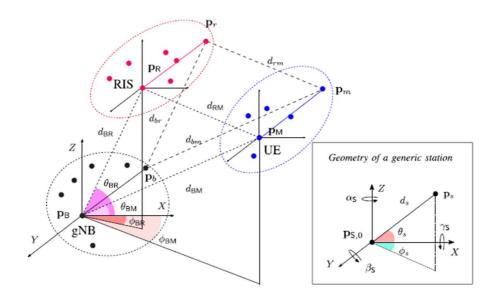

Figure 6: 3D geometry of the considered localization scenario

Considering the gNB as the center of the coordinate system, the UE and RIS centers' coordinates can be expressed as $p_S \triangleq [x_S, y_S, z_S]^T$ with $S \in \{M, R\}$ being a label for a generic station and whose coordinates are:

$$x_S = x_B + d_{BS} \cos(\theta_{BS}) \cos(\phi_{BS})$$

$$y_S = y_B + d_{BS} \cos(\theta_{BS}) \sin(\phi_{BS})$$

$$z_S = z_B + d_{BS} \sin(\theta_{BS})$$

Notably, the spherical coordinates can be easily retrieved from the equations above. Further, for each $S \in B, R, M$ and for each corresponding antenna index $s \in b, r, m$, the antenna coordinates can be indicated of each array as $pS_{,s} \triangleq p_s = [x_s, y_s, z_s]^T$ where $\forall s \in 1, 2, \dots, N_S$:

$$x_s = d_s \cos(\theta_s) \cos(\phi_s)$$

$$y_s = d_s \cos(\theta_s) \sin(\phi_s)$$

$$z_s = d_s \sin(\theta_s)$$

where N_S is the number of antennas at the considered array, and ϕ_s and θ_s are the azimuth and elevation angles of the s-th antenna element measured from the array center, respectively. In addition, arrays can be rotated around the axes, that is $\forall s \in 1, 2, \dots, N_S$, it results in:

$$\boldsymbol{p}_{S,s} = \begin{bmatrix} x_{S,s}, y_{S,s}, z_{S,s} \end{bmatrix}^T = \boldsymbol{R}(\alpha_S, \beta_S, \gamma_S) \boldsymbol{p}_{S,s}^{(0)}$$

with $\boldsymbol{p}_{S,s}^{(0)}$ being the initial array deployment, and $\boldsymbol{R}(\alpha_S, \beta_S, \gamma_S)$ is the rotation matrix given by the multiplication of the rotation matrices for each axis where $(\alpha_S, \beta_S, \gamma_S)$ are the yaw, pitch, and roll angles. The yaw, indicated with α_S, corresponds to the azimuth, as it is the rotation around the z-axis. β_S is the pitch, around the y-axis, whereas γ_S is the roll entailing a rotation around the x-axis.

A model which accounts for spherical wavefront, valid also for near-field propagation conditions, is described next. In the uplink, the UE transmits N Orthogonal Frequency-Division Multiplexing (OFDM) subcarriers, i.e. for the n-th subcarrier with $n \in \mathbb{N}_s \triangleq 1,2,\dots,N$, it results in:

$$\boldsymbol{x}[n] = \left[x_1, x_2, \dots, x_{N_M}\right]^T \triangleq \boldsymbol{w}[n]\, p[n]$$

where N_M is the number of antennas at the UE, $p[n]$ is the data symbol corresponding to the n-th subcarrier with $\mathbb{E}p[n]p*[n] = 1$, and $w[n] \in \mathbb{C}^{N_M}$ is the beamforming vector with $\parallel w[n] \parallel^2 = 1$, which can be written as:

$$\boldsymbol{w}[n] = \left[a_1\, e^{j\,\beta_1}, a_2\, e^{j\,\beta_2}, \dots, a_m\, e^{j\,\beta_m}, \dots, a_{N_M}\, e^{j\,\beta_{N_M}}\right]^T,$$

where α_m and βm represent the m-th amplitude and phase of the transmit-beamformer. Let $\Theta \triangleq \theta_1, \theta_2, \dots, \theta_{N^R}$ be the vector containing the designed phase shifts induced at the RIS, and N^R the number of RIS elements. Then:

$$\boldsymbol{\Omega} = diag(e^{j\boldsymbol{\Theta}}) \triangleq diag\left(e^{j\theta_1}, e^{j\theta_2}, \dots, e^{j\theta_{N_R}}\right),$$

Is the $N^R \times N^R$ diagonal matrix containing the RIS phases.

The gNB estimates the UE position, p_M, and its orientation, ϕ_M, by exploiting the spherical waveform model. The received signal at the gNB for the n-th subcarrier can be written as:

$$\boldsymbol{y}[n] = \sqrt{P}\, \boldsymbol{H}_{BM}[n]\, \boldsymbol{x}[n] + \sqrt{P}\boldsymbol{H}_{BR}[n]\, \boldsymbol{\Omega}\boldsymbol{H}_{RM}[n]\boldsymbol{x}[n] + \boldsymbol{\omega}[n]$$

$$\triangleq \boldsymbol{\mu}[n] + \boldsymbol{\omega}[n], \qquad \forall\, n \in \mathbb{N}_s$$

where P is the signal power, $x[n]$ is the transmitted vector for the n-th carrier frequency, $\omega[n]$ is an additive thermal noise. The channel matrices are $\mathbf{H}_{BM}[n]$, $\mathbf{H}_{RM}[n]$, and $\mathbf{H}_{BR}[n]$ for the gNB-UE, RIS-UE, and gNB-RIS links of sizes $N_B \times N_M$, $N_R \times N_M$, and $N_B \times N_R$, respectively.

In the following, it is discriminated whether the gNB and the UE have been synchronized or not. For non-synchronous systems, the position information can still be gathered from the spherical wavefront, even if no information can be retrieved from the Time of Arrival (ToA).

Synchronous System

Consider that a synchronization procedure has been performed between the gNB and the UE prior the localization step. Once synchronized, the positioning information can be retrieved by jointly processing temporal and angular information of the received signal. By extending the received signal model to its scalar notation, the general model of the received signal can be rewritten as:

$$y_b[n] = \mu_b[n] + w[n], \forall b \in \{1,2,\dots,N_B\}$$

with N_B being the number of antennas at the gNB and $w[n]$ being the circularly symmetric zero-mean Gaussian noise with power spectral density σ^2. The useful part of the signal, without the noise, is:

$$\mu_b[n] \triangleq \sqrt{P} \sum_{m=1}^{N_M} x_m[n]\, e^{-j2\pi f_n \xi_{BM}} \left(\rho_{BM} e^{-j2\pi f_n\, (\tau_{bm}+\eta_m)} + \rho_{BRM} \sum_{r=1}^{N_R} e^{j\theta_r}\, e^{-j2\pi f_n(\tau_{br}+\tau_{rm}+\eta_r+\eta_m)}\right)$$

where $f_n = f_c + n\Delta f - \frac{B}{2}$ is the frequency of the n-th subcarrier, f_c is the carrier frequency, Δf is the subcarrier spacing, $B = N\Delta f$ is the signal bandwidth, and $\tau_{bm}, \tau_{br}, \tau_{rm}$ are the delays for each couple of antenna (i.e. τbm is the delay between the b-th antenna at the gNB and the m-th antenna at the UE), ξ_{BM} is a synchronization residual (negligible after accurate synchronization procedures), and ηm and ηr are array non-idealities. The signal attenuation coefficients due to propagation are indicated with ρ_{BM} and ρ_{BRM} for the direct and the relayed path, respectively. Since the plane-wave approximation is not always valid, a spherical model is considered where the following relations hold:

$$\tau_{bm}(d_{BM}, \theta_{BM}, \phi_{BM}) = d_{bm}/c$$

$$\tau_{br}(d_{BR}, \theta_{BR}, \phi_{BR}) = d_{br}/c$$

$$\tau_{rm}(d_{RM}, \theta_{RM}, \phi_{RM}) = d_{rm}/c$$

$$\rho_{BM} = \frac{\lambda}{4\pi}\frac{1}{d_{BM}}$$

$$\rho_{BRM} = \frac{\lambda}{4\pi}\frac{1}{d_{RM}+d_{BR}}$$

where c is the speed of light, $(d_{BM}, \theta_{BM}, \phi_{BM})$, $(d_{BR}, \theta_{BR}, \phi_{BR})$ and $(d_{RM}, \theta_{RM}, \phi_{RM})$ are the distances and angles between the gNB-UE, gNB-RIS, RIS-UE centers, respectively, and where:

$$d_{bm} = \sqrt{d_m^2 + d_b^2 + d_{BM}^2 - 2\left(G_{bm}^{(1)} + d_{BM}\, G_{bm}^{(2)}\right)},$$

with $G_{bm}^{(1)}$ and $G_{bm}^{(2)}$ containing the information about the geometry at the transmitter and at the receiver, that is:

$$G_{bm}^{(1)} = x_b\, x_m + y_b\, y_m + z_b\, z_m,$$

$$G_{bm}^{(2)} = (x_m - x_b)\cos\theta_{BM}\cos\phi_{BM} + (y_m - y_b)\times\cos\theta_{BM}\sin\phi_{BM} + (z_m - z_b)\sin\theta_{BM}.$$

The distances of arrival between the b-th gNB antenna and the r-th RIS antenna and between the r-th RIS antenna and the m-th UE antenna, namely d_{br} and d_{rm}, can be found using the above definition with appropriate substitutions.

Differently from traditional schemes that make the assumption of incident planar wavefront, it is inferred jointly the ranging and bearing information from the spherical waveform curvature. Notably, it is possible to write the useful part of the signal without the noise only when the clocks of the gNB, RIS and UE have been synchronized. Note that the accurate synchronization might entail several and long procedures. In the following, an asynchronous alternative is considered where it is still possible to retrieve the UE position from the relative phases.

Asynchronous System

As evidenced in the general received signal model, from the received signal it is possible to infer the ToA estimate, which is possible in all those situations where a synchronization procedure has been performed. In this case, the system is no more able to directly estimate the information of the distance from the ToA. Instead, the incident waveform curvature, i.e.:

$$\Delta d_{bm} = d_{bm} - d_{BM} = c\,\Delta\tau_{bm}$$

$$\Delta d_{br} = d_{br} - d_{BR} = c\,\Delta\tau_{br}$$

can be exploited for UE localization since it holds:

$$y_b[n] = \sqrt{P}\sum_{m=1}^{N_M} x_m[n]\Big(\rho_{BM}\, e^{-j\chi_{BM}}\, e^{-j2\pi f_n\,(\Delta\tau_{bm}+\eta_m)} + \rho_{BRM}e^{-j\chi_{BRM}}\sum_{r=1}^{N_R} e^{j\theta_r}e^{-j2\pi f_n(\Delta\tau_{br}+\Delta\tau_{rm}+\eta_r+\eta_m)}\Big) + w[n],\Big)$$

where χ_{BM} and χ_{BRM} are uniformly distributed random variables between 0 and 2π representing the phase offsets between the gNB, the UE and the RIS due to the lack of synchronization.

5.2.3   Far-field

Figure 7 shows the same SISO setup but with the BS and UE being in the far field of the RIS, where the distance between the UE and BS is much larger than the RIS size.
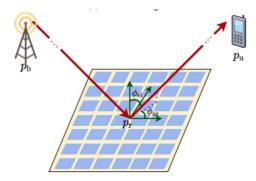

Figure 7: The far-field regimes of the RIS-enabled signal propagation with respect to the RIS

In this case, the wireless channel can be described by the AoD, which consists of elevation and azimuth factors (represented by Φ_{el} and Φ_{az}).

The observation during the t-th reception slot ($t = 1, 2,..., T$) at the m-th RIS's RX RF chain output can be mathematically expressed as follows:

$$y_{m,t} = \boldsymbol{u}_{m,t}^H \sum_{c=1}^{C_m} h_{m,c} \, \boldsymbol{\alpha}\big(\Phi_{m,el}, \Phi_{m,az}\big) s + \boldsymbol{u}_{m,t}^H \boldsymbol{w}_{m,t}$$

where the spatial response vector $\boldsymbol{\alpha}\big(\Phi_{m,el}, \Phi_{m,az}\big) \in \mathbb{C}^{L \times 1}$ for the azimuth and elevation Angle of Arrivals (AoA) $\Phi_{m,el} \in [0,\pi]$ and $\Phi_{m,az} \in [0,2\pi]$, respectively, of the user transmitted signal via multipath propagation, with respect to the coordinate system having as origin the point $\mathbf{p}_m$ (i.e. the reference point of the m-th RIS), is given for $l = 1, 2,..., L$ as follows:

$$\big[\boldsymbol{\alpha}\big(\Phi_{m,el}, \Phi_{m,az}\big)\big]_l = \boldsymbol{exp}\left(-j\mathbf{q}_{m,l}^T \mathbf{k}\big(\Phi_{m,el}, \Phi_{m,az}\big)\right)$$

where $\mathbf{q}_{m,l}$ denotes the position of the l-th element of the m-th RIS and $\mathbf{k}\big(\Phi_{m,el}, \Phi_{m,az}\big)$ is the wavevector at these respective AoAs, which is mathematically defined as:

$$\mathbf{k}\big(\Phi_{m,el}, \Phi_{m,az}\big) = -\frac{2\pi}{\lambda} \begin{bmatrix} \boldsymbol{sin}\,\Phi_{m,az}\,\boldsymbol{cos}\,\Phi_{m,el} \\ \boldsymbol{sin}\,\Phi_{m,az}\,\boldsymbol{sin}\,\Phi_{m,el} \\ \boldsymbol{cos}\,\Phi_{m,az} \end{bmatrix}$$

with λ as the signal wavelength.

5.3 Continuous and discrete models

RIS can reflect the impinging signal to the desired receiver, by introducing the phase-shifts and amplitude gains at each of the RIS elements. Based on the achievable resolution of the phase-shift and amplification gain, the RIS-aided channel models can be classified as the continuous and discrete models. When each of the RIS element can achieve any phase level in the range ($0-2\pi$) and amplification level (0-A), where A is the maximum achievable amplitude, the RIS model can be classified as a continuous model. The continuous model can configure the phase-shifts and amplification with infinite resolution at each RIS element. However, in many practical scenarios, the infinite resolution of the continuous RIS model may be hard to realize due to hardware limitations. Hence, the discrete models may be considered, wherein the overall achievable phase-shift and amplification gain can be discretized into a finite number of phase-shift and amplification levels respectively. Based on this classification, the designed channel models for RIS-aided communication should be designed to support the effect of continuous and discrete models. It is inherent that the channel estimation methods in the RIS-aided communication will also be impacted by the continuous and discrete models and such an effect should be studied.

One of a typical use of discrete RIS is discrete Holographic Multiple Input Multiple Output Surface (HMIMOS), which is usually composed of many discrete unit cells made of lowpower and software-tuneable metamaterials. In order to modify the electromagnetic properties of the unit cells, the materials are typically chosen from electronic components that are off the shelves to liquid crystals, microelectromechanical systems or even electromechanical switches, and other reconfigurable metamaterials. This structure is substantially different from conventional MIMO antenna arrays. One embodiment of a discrete surface is based on discrete "meta-atoms" with electronically steerable reflection properties. Another type of discrete surface is the active RIS based, i.e. on photonic antenna arrays. It integrates active optical-electrical detectors, converters, and modulators for performing transmission, reception, and conversion of optical or RF signals. Contiguous RIS can form a spatially continuous transceiver aperture by integrating a virtually number if elements into a limited surface area.

6 Channel models

6.1 Objectives of channel modeling and general principles

The channel models developed and characterized in this clause mainly serve the following needs:

- Provide building blocks for studies in the present document or other reports of ISG RIS, including the analysis of interference.

- Coupled with the modeling of RIS, to provide a communication model for performance evaluation.

When modeling the channel, different frequency ranges, bandwidth and the modeling of RIS elements need to be taken into account.

It should be noted that channel modeling usually involves a trade-off between complexity and accuracy. For instance, in most ray-tracing based channel modeling approaches, if only single reflection is considered the model is simpler while may not be perfectly accurate. On the other hand, higher order reflections, which can characterize a more accurate channel model, are time consuming to compute and simulate. In this clause, simple models that account for only a single reflection by the RIS are considered, which means at most one RIS is considered in the propagation path between the receiver and the transmitter. Also, cascaded channels where more than one RIS exist in the propagation path between the receiver and the transmitter are studied.

6.2   Existing channel models

Channel models for different scenarios have been proposed in ETSI TR 138 901 [i.2], which can also be applied to model each hop of a RIS link (i.e. BS-RIS, RIS-UE, etc.), as illustrated in Table 1.

Table 1: 3GPP channel models that are applicable to RIS use cases

Scenarios	BS-UE channel model	BS-RIS channel model	RIS-UE channel model	RIS-RIS channel model
Urban deployment: avoiding indoor UE's penetration loss	Uma/Umi	Uma/Umi	InH/InF	Uma/Umi/InH/InF
Urban deployment: UE-controlled RIS	Uma/Umi	Uma/Umi	LOS	N/A
Urban deployment: RIS close to BS	Uma/Umi	LOS	Uma/Umi	Umi
Urban deployment: coverage extension	Uma/Umi	Uma/Umi	Uma/Umi	Uma/Umi
Indoor scenario	InH/InF	InH/InF/LOS	InH/InF/LOS	InH/InF

In urban scenarios, the BS-RIS channel model can generally be modeled using Uma/Umi models, dependent on the network deployment (i.e. the height of BS/RIS). The RIS-UE channel can be modeled with InH/InF is the link is indoor or modeled with Uma/Umi otherwise. If the distance between RIS and UE or between BS and RIS is very small, a pure LOS channel model is applicable. RIS-RIS channels can be utilized when multiple RIS are utilized in the same link in a cascaded manner. In O2I use cases, the RIS-RIS channel can be either outdoor or indoor; for coverage extension, the RIS-RIS channel need to be modeled by Uma/Umi channel models.

6.3   Path-loss models

6.3.1   Description of different cases

6.3.1.1   General description

The electric and magnetic fields behave differently in the near-field (Fresnel) and far-field region. Hence, near-field requires a different path-loss model than the far-field. In addition, the path-loss model of the near-field need to consider both high frequency and low frequency ranges. Since the near-field region depends on the frequency (or wavelength) and array size, near-field conditions may occur not only in short-range scenarios, but also in mid-range scenarios.

6.3.1.2   General case

The free-space path loss of a BS-RIS-UE cascaded channel can generally be modeled as [i.6] and [i.7]:

$$PL = \frac{64\pi^3}{G_t G_r G d_x d_y \lambda^2} \times \frac{1}{\left| \sum_{m=1}^{M} \sum_{n=1}^{N} \frac{\sqrt{F_{n,m}} \Gamma_{n,m}}{r_{n,m}^t r_{n,m}^r} e^{\frac{-j2\pi(r_{n,m}^t + r_{n,m}^r)}{\lambda}} \right|^2}$$

which is a general formula valid for both far-field and near-field. Here G_t and G_r represent the transmit and receive antenna gain, and G represents the scattering gain of a single RIS element. d_x and d_y represent the width and length of each RIS element. The RIS is assumed to have $M \times N$ elements in total. The terms $r_{n,m}^t$ and $r_{n,m}^r$ are the distances from each RIS element to the transmitter and the receiver, respectively. $F_{n,m}$ is the combined power radiation pattern of transmitter, receiver, and RIS. $\Gamma_{n,m}$ is the reflection coefficient of each RIS element. The wavelength of the carrier frequency is represented by λ. A common assumption of RIS element scattering gain is that $G = \frac{4\pi d_x d_y}{\lambda^2}$, which is the recommended [i.7]. This path-loss model is obtained under the assumption of locally periodic discrete model for the RIS.

6.3.1.3 Near-field case

In the near-field case, the contributions from different phased array elements need to be modeled separately in terms of distances and phase shifts. Recently, a model for the path-loss of RIS in the near-field has been proposed based on measurements [i.6]. In this study, the near-field path-loss model is expressed as a function of the transmit power, the gain of the RIS elements, the square of the wavelength, and the received power. In addition, this study indicates that the received power is related to the normalized power radiation patterns of the transmitting/receiving antennas and RIS elements, the reflection coefficients of the RIS elements, and the distances between the transmitter/receiver and the RIS elements.

When the transmitter and/or receiver are in the near field of the RIS, two different RIS reflection patterns can be assumed for path loss modeling [i.7]. When the RIS reflection coefficients are configured to broadcast signals in a desired direction, an approximate expression of the near-field path-loss model is proposed in [i.6]:

$$PL_{\mathrm{nf}} \approx \frac{1}{G_t G_r} \left[\frac{4\pi(d_t + d_r)}{\lambda A} \right]^2$$

where G_t, G_r is the transmit/receive gain respectively, λ denotes the wavelength, A is the maximum gain of RIS element, d_t and d_r represent the distance between the transmitter/receiver and the center of RIS. This approximated near-field path-loss expression in [i.6] is aligned with the path-loss model proposed [i.8] when considering an RIS which is oriented such that Snell's law of reflection (i.e. the angle of reflection is equal to the angle of incidence) is satisfied at the RIS and the size of RIS array is assumed to be infinite. Based on this model, the near-field path loss for near-field broadcasting is equal to that of a free-space path with a total distance given by the sums of the TX-RIS and RIS-RX distances. This approximated path-loss model is useful as a starting reference and the actual path-loss can be obtained with a modified or correction term. A general discussion about the validity of this approximated near-field path-loss model is reported in [i.9], where it is shown that it can be applied under some specific propagation conditions and configurations of the RIS, which, however, are not limited to the conventional Snell law of reflection.

EXAMPLE: It is shown to hold if the RIS is configured as an anomalous reflector introducing a linear phase shift as a function of the angle of incidence and reflection.

If, on the other hand, the optimal RIS reflection coefficients are configured to focus the signal at the receiver, the path-loss of the cascaded channel in the near-field can be modeled as [i.7]:

$$PL = \frac{64\pi^3}{G_t G_r G d_x d_y \lambda^2 A^2 \left| \sum_{m=1}^{M} \sum_{n=1}^{N} \frac{\sqrt{F_{n,m}}}{r_{n,m}^t r_{n,m}^r} \right|^2}.$$

where the definitions of the parameters are the same as those for the general case.

6.3.1.4 Far-field case

When the transmitter is sufficiently far away from the receiver, the spherical wave generated by the transmitter can be approximated by a plane wave at the receiver side, and different phased array elements can be modeled in a single entity, as far as the distance is concerned, while the phases need to be modeled separately. In this case, the receiver is in the far field of the transmitter. The boundary of the far field and near field is defined as the Fraunhofer distance. In the far-field scenario, if the signals reflected by all the RIS elements are aligned in phase to enhance the received signal power, the path-loss can be approximated as:

$$PL = \frac{64\pi^3 (d_t d_r)^2}{G_t G_r G (MN)^2 d_x d_y \lambda^2 F(\theta_t, \phi_t) F(\theta_r, \phi_r) A^2}.$$

where d_t and d_r represent the distance between the transmitter/receiver and the center of RIS. $F(\theta_t, \phi_t)$ is the normalized radiation pattern of each RIS element to the transmitter, in which θ_t and ϕ_t represent the elevation angle and azimuth angle from the center of the RIS to the transmitter. Similarly, $F(\theta_r, \phi_r)$ is the normalized radiation pattern to the receiver's direction. The variable A is the amplitude of reflection coefficients of each RIS element, which is assumed to be the same for all the RIS elements. This far-field path loss calculation is based on the free-space path loss model.

6.4   Empirical channel model

A supplementary channel model incorporating an extra component related to RIS relaying performance is described in this clause. To this end, two different cases are considered. In the first case, the signal propagates through available links in the environment without using RIS, and the corresponding channels are measured. In the second case, an RIS within the propagation environment is deployed, and the channels between transceivers are measured. By comparing these two cases, it is possible to dedicate an extra parameter to the impact of the RIS impact introduce a new extended 3GPP channel model taking the RIS into account. To do so, the 3GPP 5G NR model for channel path loss as the basic model where no RIS are deployed within the propagation environments is adopted, see ETSI TR 138 901 [i.2]. In the second step, an RIS in an indoor and outdoor environment is deployed, and consider an extra component dedicated to the RIS impact.

When no RIS is present, the corresponding channel model between the transmitter and receiver is:

$$L^{T-R}(f) = -20\log_{10}\left(\frac{4\pi}{\lambda}\right) - 10l\left(1 + \eta\left(\frac{f - f_0}{f_0}\right)\right)\log_{10}(d) - X_\sigma$$

where $d \approx b + c$ is the direct distance between the transmitter and the receiver with b and c being the distance between the transmitter and RIS centroid and the distance between the RIS centroid and the receiver, respectively.

On the other hand, the equivalent channel path loss between the transmitter and receiver in presence of an RIS is:

$$L_{eq}^{T-R} = L^{T-R} + L_{ref}^{RIS} + g(f_0, l_{eq}, \eta_{eq}, b, c)$$

where L_{ref}^{RIS} denotes the RIS reflection loss which is assumed to be known in the measurement. In this formula, $g(f_0, l_{eq}, \eta_{eq}, b, c)$ is modeled as follows:

$$g(f_0, l_{eq}, \eta_{eq}, b, c) = 10l_{eq}\left(1 + \eta_{eq}\left(\frac{f - f_0}{f_0}\right)\right)\log_{10}(b + c)$$

To be specific, the aim is to obtain appropriate parameters for $g(f_0, l_{eq}, \eta_{eq}, b, c)$, i. e., l_{eq} and η_{eq}, which are able to well characterize the impacts of the RIS on the channel attenuation and path loss. To do so, the transceiver channels in the absence of RIS is measured. Then, the RIS is deployed and the measurements are repeated. Comparing these measurements, the parameters can be estimated. The results are reported in Table 2 and Table 3 for directional horn antennas and hybrid antennas, i.e. directional at the transmitter and omni-directional at the receiver.

Table 2: Path loss parameters for directional antennas

Parameter	InH Indoor (NLOS)	UMi Outdoor (NLOS)
l	2,15	2,2
σ	6,68 dB	6,81 dB
η	0,01	0,01
l_{eq}	1,7	1,6
η_{eq}	0,01	0,01

Table 3: Path loss parameters for omni-directional antennas

Parameter	InH Indoor (NLOS)	UMi Outdoor (NLOS)
l	2,31	2,28
σ	6,79 dB	6,91 dB
η	0,01	0,01
l_{eq}	1,78	1,7
η_{eq}	0,01	0,01

6.5   Multipath models

6.5.1   Unstructured models for rich scattering (sub-6 GHz) environments

In sub-6 GHz band, the multipath can be modeled using stochastic models given the rich scattering (i.e. isotropic scattering) environment. The fading channel of each hop can be modeled using correlated Rayleigh of Rician fading models. Under the assumption of Rayleigh fading, the channel vector coefficients are complex Gaussian random variables with 0 mean and covariance matrix $d_x d_y \mu R$, where $d_x d_y$ is the size of RIS element and μ is the average intensity attenuation. The (n, m) element of the spatial correlation matrix $\boldsymbol{R}$ is [i.10]:

$$[R]_{n,m} = sinc\left(\frac{\|u_n - u_m\|}{\lambda}\right)$$

where $\boldsymbol{u_n}$ denotes the location of the nth element of RIS. The multipath Rayleigh fading will only be i.i.d. Rayleigh fading if $\boldsymbol{R}$ is an identity matrix.

If a Rician fading model is considered, two different approaches can typically be utilized.

- **Multiplicative models:** In this case, the impact from surrounding scatterers is taken into account in both links between the transmitter and the RIS and between the RIS and the receiver. In general, the end-to-end channel model can be written as follows [i.11]:

$$\mathbf{H} = \mathbf{H}_{\mathrm{DIR}} + \mathbf{H}_{\mathrm{INDIR}}$$

where the first addend is the direct channel and the second addend is the indirect channel. The latter term includes the impact of the RIS and is formulated as:

$$\mathbf{H}_{\mathrm{INDIR}} = \sqrt{\beta_{\mathrm{INDIR}}^{-1}} \mathbf{H}_2 \mathbf{F}(\theta) \mathbf{H}_1$$

where the multiplying scaling factor accounts for the path-loss, $\mathbf{H}_1$ is the channel matrix from the transmitter to the RIS, $\mathbf{H}_2$ is the channel matrix from the RIS to the receiver, and $\mathbf{F}$ models the response of the RIS. Both channels $\mathbf{H}_1$ and $\mathbf{H}_2$ are assumed to follow a Rician distribution, which can include spatial correlation as well.

- **Additive models**. In this case, multipath propagation from surrounding scatterers is taken into account by viewing the RIS as additional digitally controllable scatterers and second-order scattering effects are ignored. In this case, the RIS-aided channel is modeled as follows [i.12]:

$$\mathbf{H} = \mathbf{H}_{\mathrm{DIR}}^{\mathrm{FS}} + \mathbf{H}_{\mathrm{INDIR}}^{\mathrm{FS}} + \mathbf{H}^{\mathrm{MPC}}$$

where the first addend accounts for the direct link in free-space, the second added for the RIS-reflected link assuming that both constituent links are in free-space, and the last addend accounts for the surrounding multipath propagation, which can be modeled by using standard channel models.

6.5.2   Structured models for rich scattering (sub-6 GHz) environments

The multipath of an RIS link can also be modeled using cluster-based method [i.13]. In the far-field scenario, if the BS-RIS and RIS-UE path has C clusters (each cluster has S rays), the channel of this hop can be modeled as:

$$\boldsymbol{h} = \sum_{c=1}^{C} \sum_{s=1}^{S} \sqrt{\frac{P_c}{S}} \sqrt{\frac{G_e(\theta_{c,s}, \phi_{c,s})}{P_L}} e^{j\Phi_{c,s}} \boldsymbol{a}(\theta_{c,s}, \phi_{c,s})$$

where $\boldsymbol{a}(\theta_{c,s}, \phi_{c,s})$ is the array response vector of RIS for azimuth angle $\phi_{c,s}$ and elevation angle $\theta_{c,s}$, and G_e is the RIS antenna element pattern. P_c is the power of each cluster, while P_L is the path loss component. $\boldsymbol{\Phi}_{c,s}$ represents the random phase of each ray (c, s). When the link is LOS, the path of the first cluster is viewed as the LOS path and the LOS power component is added to P_c. In the near-field scenario, pure LOS links are usually assumed. The BS-UE path can be similarly modeled without considering the departure and arrival angles:

$$h^{BU} = \sum_{c=1}^{C} \sum_{s=1}^{S} \sqrt{\frac{P_c}{S}} \sqrt{\frac{1}{P_L}} e^{j\Phi_{c,s}}$$

6.5.3 Structured (geometric) models for high frequency bands

An example strategy proposed in [i.13] models the multipath of an RIS link using a cluster-based method. When the RIS is not close enough to the BS/UE, the clusters and rays for BS-RIS, RIS-UE, and BS-UE paths need to be modeled separately. When the RIS is close to UE, the clusters and rays for BS-UE path should be reused for the BS-RIS path. If the BS-RIS and RIS-UE path has C clusters (each cluster has S_c rays), the channel of this hop can be modeled as:

$$h = \gamma \sum_{c=1}^{C} \sum_{s=1}^{S_c} \beta_{c,s} \sqrt{G_e(\theta_{c,s}, \phi_{c,s})L} \, a(\theta_{c,s}, \phi_{c,s}) + h_{LOS}$$

where γ is a normalization factor, $\beta_{c,s}$ is the complex Gaussian distributed path gain, and L is the path loss. The existence of LOS component $\boldsymbol{h_{LOS}}$ is probabilistic, and if it exists, the LOS channel can be modeled as:

$$\boldsymbol{h_{LOS}} = e^{j\eta} \sqrt{G_e(\theta_{LOS}, \phi_{LOS})L} \, \boldsymbol{a}(\theta_{LOS}, \phi_{LOS})$$

where η is a random phase term. The BS-UE path can be similarly modeled without considering the departure and arrival angles:

$$h^{BU} = \gamma \sum_{c=1}^{C} \sum_{s=1}^{S_c} \beta_{c,s} e^{j\eta} \sqrt{L} + h_{LOS}^{BU}$$

As a general model for structured channels, the Saleh-Valenzuela model [SV-1978], [i.14] can be utilized.

6.6 Multi-mode reradiation models

Depending on how an RIS is realized, it can reradiate multiple waves for a given incident electromagnetic wave [i.16]. These unwanted scattered waves are considered as interference (undesired effects) in wireless communications. A model that captures this behaviour is the following [i.17]:

$$\Gamma(x', y') = \sum_{n} \Gamma_n = R \sum_{n} \sqrt{m_n} A_{m_n}(x', y') \exp(j\chi_{m_n}(x', y'))$$

where the variable m_n denotes the amount of power that is scattered by the nth mode, while the factor A(.) and X(.) determine the phase modulation for each of the scattered mode. If the scattered waves are plane waves, A(.) is a constant term that is the same for each element of the RIS.

Based on this multi-mode reradiation model, the scattered electromagnetic field can be formulated as follows:

$$\mathbf{E}_n(P) = \iint_{S_{RIS}} j \frac{e^{-jkr''}}{\lambda r''} \left[\hat{\mathbf{r}}'' \times (\eta \hat{\mathbf{n}} \times \mathbf{H}_a(x', y')) \times \hat{\mathbf{r}}'' \right] dS + \iint_{S_{RIS}} j \frac{e^{-jkr''}}{\lambda r''} \left[\hat{\mathbf{r}}'' \times (\mathbf{E}_a(x', y')) \times \hat{\mathbf{n}} \right] dS$$

where:

$$\mathbf{E}_a(P') = -\frac{1 - \Gamma(P')}{2} \mathbf{E}_{it}(P')$$

$$\mathbf{H}_a(P') = \frac{1 + \Gamma(P')}{2} \mathbf{H}_{it}(P')$$

and

$$\mathbf{E}_{it}(P') = \hat{\mathbf{n}} \times (\mathbf{E}_i(P') \times \hat{\mathbf{n}})$$

$$\mathbf{H}_{it}(P') = \hat{\mathbf{n}} \times (\mathbf{H}_i(P') \times \hat{\mathbf{n}})$$

where the symbols are defined in Figure 8 and $\mathbf{E_i}$ and $\mathbf{H_i}$ are the incident electric and magnetic fields. Specially, $\Gamma(.)$ denotes the point-wide reflection coefficient of the RIS.
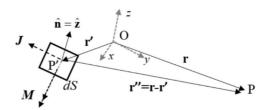

Figure 8: Notation for multi-mode reradiation

6.7   Interference and unwanted reradiation models

6.7.1   Definition of interference and unwanted reradiation

6.7.1.1   General description

In the context of RIS-aided communications, interference can be categorized as follows:

- **Generated by the RIS itself:** This refers to the spurious signals generated by the RIS due to its inherent structure. For example, the multi-mode propagation model accounts for this effect.

- **Generated by other RIS:** This refers to the interference generated by other RIS devices in the network.

- **Single operator modeling:** This refers to the modeling of interference in single-operator networks.

- **Multi/inter-operator modeling:** This refers to the modeling of interference in inter- operator networks.

- **Eavesdropping:** This refers to case studies including security.

In the present clause, the most general definition of interference and unwanted reradiations due to RIS is provided. In the context of this general definition, there is no constraint on the way the RIS is controlled.
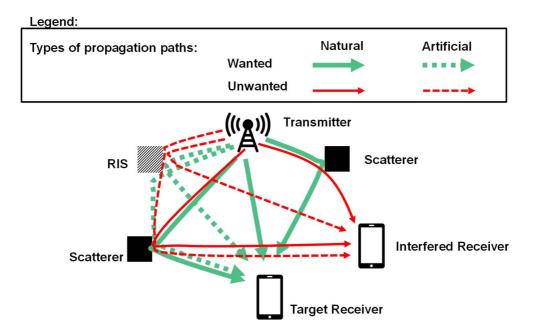
6.7.1.2   RIS contribution to the interference propagation channel (In-Band Reradiation)

In wireless networks without RIS, the following types of in-band interference already exist:

- Multi-user interference.

- Multi-cell interference.

Introducing an RIS in wireless networks not only has an impact on the propagation channel between a transmitter and its target receiver. It also has an impact on the propagation channel between a transmitter and its interfered receiver: i.e. the interference propagation channel. In the present clause, it is proposed to define the contribution of RIS to this interference propagation channel.

As illustrated in Figure 9, a link between a transmitter and a target receiver is considered, in the presence of a RIS participating to the communication between the transmitter and the target receiver.

Figure 9: Artificial Propagation Paths due to RIS, potentially adding interference

Figure 9 shows an interfered receiver as well. Finally, it is assumed that all the following frequency bands do overlap:

- The frequency band used by the communication link between the transmitter and the target receiver.

- The bandwidth of influence of the RIS.
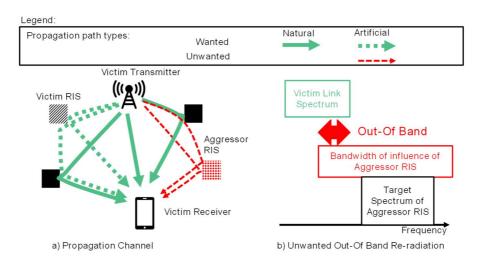
- The frequency band used by the interfered receiver.

Such scenario can happen, typically, in multi-user transmission, where the transmitter simultaneously serves two receivers (in a multi-user configuration) and RIS is tuned with the aim of focusing towards the target receiver and avoiding the interfered user. Such scenario can also happen in a multi-cell configuration, where the considered transmitter serves the target receiver, and the interfered receiver is served by another transmitter (not represented in the figure) but is located in the coverage area (typically at the border) of the first transmitter. Hence, in such scenarios, only the in-band unwanted reradiation by the RIS is studied. The out-of-band unwanted reradiation is studied in clause 6.7.1.3.

Specifically, the figure illustrates the case where the RIS is tuned to serve the target receiver and creates several additional temporary "artificial" propagation paths between the transmitter and the interfered receiver. These paths may potentially induce In-Band Reradiation (i.e. mainlobe and sidelobes) of the signal that is only intended for the target receiver and not for the interfered receiver. This can be seen as a contribution of the RIS to the total interference received at the interfered receiver due the sidelobes of RIS reflected beam. Depending on the implementation of the RIS and the implementation of the network, this contribution of RIS can have an unwanted impact (i.e. that the contribution of the RIS adds up to the total interference due to "natural" propagation paths between the transmitter and the interfered receiver) or a desired impact (i.e. the contribution of the RIS reduces the total interference between the transmitter and the interfered receiver).

In the context of this general definition, any constrain on the definition of an unwanted propagation path is put. In practice, it can be "one hop" path (from the transmitter to the receiver through one RIS element), a "multi-hop" path (i.e. going through one RIS element and one or several scatterers).

6.7.1.3   Unwanted reradiations (Unexpected/Irregular/Discontinuously Time-Varying Out-Of-Band Reradiation)

As illustrated in Figure 10 (sub-figure a)), a victim link between a victim transmitter and a victim receiver is considered, aided by an RIS, and in the presence of an aggressor RIS which is not controlled by the victim network (the victim network including, the victim transmitter, the victim receiver and the aiding RIS).

**Figure 10: Artificial Propagation Path due to aggressor RIS,
potentially creating unwanted fluctuations in the propagation channel**

It is assumed that all the following frequency bands do overlap (as illustrated in Figure 10 sub-figure b)):

- The frequency band used by the communication link between the transmitter and the target receiver.

- The bandwidth of influence of the aggressor RIS.

Hence, in this scenario, only the out-of-band unwanted reradiation by the aggressor RIS is studied. The in-band unwanted reradiation is discussed next.

Figure 15 illustrates the case where the RIS is tuned to serve the target receiver and creates several additional temporary "artificial" propagation paths between the transmitter and the interfered receiver. Depending on the level of knowledge that the victim nodes may have regarding the aggressor RIS configuration, these paths may potentially induce unpredictable Discontinuous Time-Variations of the propagation channel between the victim transmitter and the victim receiver when RIS is reconfigured according to the requirement of the target receiver. Different from the case of in-band reradiation, the victim operator and the victim receiver cannot predict of the aggressor RIS reconfiguration. This degradation in the predictability of the propagation channel may potentially degrade closed-loop link adaptation mechanisms. In that sense, the aggressor link is potentially creating unwanted re-radiations.

In the context of this general definition, any constrain on the definition of an unwanted propagation path is put. In practice, it can be "one hop" path (from the transmitter to the receiver through one RIS element), a "multi-hop" path (i.e. going through one RIS element and one or several scatterers).

6.7.2   Characterization of interference and unwanted reradiation

6.7.2.0   General description

The unwanted self-reradiation (interference) from an RIS can be modeled as detailed in clause 7.6 (multi-mode reradiation models). This source of interference is not considered in this clause.

The signal and interference power of RIS links can be modeled in the example scenario shown in Figure 11.
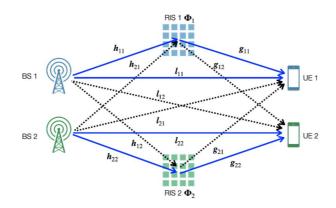
Figure 11: Example scenario - Two links aided by two RIS

Two links, BS1-UE1 and BS2-UE2 aided by RIS, are considered. The transmit powers of BS1 and BS2 are represented by P_1 and P_2. The reflection coefficients of RIS1 and RIS2 are represented by $\boldsymbol{\Phi}_1$ and $\boldsymbol{\Phi}_2$. The channels between each pair of BS and RIS are $\{\boldsymbol{h}_{11}, \boldsymbol{h}_{12}, \boldsymbol{h}_{21}, \boldsymbol{h}_{22}\}$. The channels between each pair of RIS and UE are $\{\boldsymbol{g}_{11}, \boldsymbol{g}_{12}, \boldsymbol{g}_{21}, \boldsymbol{g}_{22}\}$. The channels between each pair of BS and UE without the aid of RIS are $\{\boldsymbol{l}_{11}, \boldsymbol{l}_{12}, \boldsymbol{l}_{21}, \boldsymbol{l}_{22}\}$. The beamforming effects of BS and UE are integrated into the channels to simplify the notation.

Assuming a narrow band channel model, the received signal strength at UE1 and UE2 can be modeled as:

$$S_1 = P_1 |\boldsymbol{h}_{11}\boldsymbol{\Phi}_1\boldsymbol{g}_{11} + \boldsymbol{h}_{12}\boldsymbol{\Phi}_2\boldsymbol{g}_{21} + \boldsymbol{l}_{11}|^2$$

$$S_2 = P_2 |\boldsymbol{h}_{21}\boldsymbol{\Phi}_1\boldsymbol{g}_{12} + \boldsymbol{h}_{22}\boldsymbol{\Phi}_2\boldsymbol{g}_{22} + \boldsymbol{l}_{22}|^2$$

And the total interference for each UE can be modeled as:

$$I_1 = P_2 |\boldsymbol{h}_{21}\boldsymbol{\Phi}_1\boldsymbol{g}_{11} + \boldsymbol{h}_{22}\boldsymbol{\Phi}_2\boldsymbol{g}_{21} + \boldsymbol{l}_{21}|^2$$

$$I_2 = P_1 |\boldsymbol{h}_{11}\boldsymbol{\Phi}_1\boldsymbol{g}_{12} + \boldsymbol{h}_{12}\boldsymbol{\Phi}_2\boldsymbol{g}_{22} + \boldsymbol{l}_{12}|^2$$

For each UE, the interference can be generated by the configured RIS of the current link, by other RIS, or without RIS.

6.7.2.1   Generated by the RIS itself

The interference signal to UE1 generated by RIS1 is $\sqrt{P_2}\boldsymbol{h}_{21}\boldsymbol{\Phi}_1\boldsymbol{g}_{11}$, and the interference signal to UE2 generated by RIS2 is $\sqrt{P_1}\boldsymbol{h}_{12}\boldsymbol{\Phi}_2\boldsymbol{g}_{22}$. In some other scenarios, interference can also be generated when a transmitter's signal is required to be reflected to multiple receivers in a multi-mode reradiation manner.

6.7.2.2   Generated by other RIS

The interference signal to UE1 generated by RIS2 is $\sqrt{P_2}\boldsymbol{h}_{22}\boldsymbol{\Phi}_2\boldsymbol{g}_{21}$, and the interference signal to UE2 generated by RIS1 is $\sqrt{P_1}\boldsymbol{h}_{11}\boldsymbol{\Phi}_1\boldsymbol{g}_{12}$. The SNRs of UE1 and UE2 are $SNR_1 = \frac{S_1}{N_1}$ and $SNR_2 = \frac{S_2}{N_2}$. The SINRs of UE1 and UE2 are $SINR_1 = \frac{S_1}{N_1+I_1}$ and $SNR_2 = \frac{S_2}{N_2+I_2}$. The rate of the two RIS aided BS-UE links can be calculated with $C_1 = B\log_2(1 + SINR_1)$ and $C_2 = B\log_2(1 + SINR_2)$.

6.7.2.3   Single and Multi/Inter-Operator Modeling

The signal and interference modeling in the single-operator and multi/inter-operator scenarios is different due to the different capability of coordination. If two links are managed by the same operator, different transmitters and RIS can be jointly optimized to reduce the potential interference and optimize the total capacity. i.e. theoretically the RIS reflection coefficients $\boldsymbol{\Phi}_1$ and $\boldsymbol{\Phi}_2$ can be jointly optimized as:

$$\{\boldsymbol{\Phi}_1, \boldsymbol{\Phi}_2\} = \arg\max_{\boldsymbol{\Phi}_1, \boldsymbol{\Phi}_2} C_1 + C_2$$

If one link is not scheduled in a certain frame, RIS that are not configured can also be temporarily turned off to reduce interference. In realistic scenarios, such joint optimization requires shared channels and RIS information between cells and may not always be supported.

In multi/inter-operator scenario, the RIS reflection coefficients $\boldsymbol{\Phi}_1$ and $\boldsymbol{\Phi}_2$ can only be separately optimized without the knowledge of the other link, i.e.:

$$\boldsymbol{\Phi}_1 = \arg\max_{\boldsymbol{\Phi}_1} P_1 |\boldsymbol{h}_{11}\boldsymbol{\Phi}_1\boldsymbol{g}_{11} + \boldsymbol{l}_{11}|^2$$

$$\boldsymbol{\Phi}_2 = \arg\max_{\boldsymbol{\Phi}_2} P_2 |\boldsymbol{h}_{22}\boldsymbol{\Phi}_2\boldsymbol{g}_{22} + \boldsymbol{l}_{22}|^2$$

In this case, the signal of link BS1-UE1 reflected by RIS2 is not considered in the optimization of $\boldsymbol{\Phi}_1$, and vice versa, which may end up as destructive components for the received signal power. In addition, the interference cannot be minimized by tuning the RIS configuration in multi/inter-operator scenario.

6.7.2.4   Eavesdropping

Eavesdroppers can take the advantage of RIS to receive the signals sent to the intended receiver, even without a direct link to the transmitter, as shown in Figure 12.
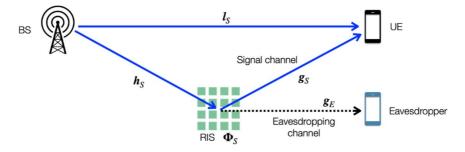

Figure 12: Eavesdropping leaked signal from RIS

Assuming a narrow band channel model, the RIS-aided rate between the transmitter and the legitimate receiver is:

$$C_S = B \log_2\left(1 + \frac{P_S|\boldsymbol{h}_S\boldsymbol{\Phi}_S\boldsymbol{g}_S + l_S|^2}{N_S}\right)$$

The rate to the eavesdropper can be modeled as:

$$C_E = B \log_2\left(1 + \frac{P_S|\boldsymbol{h}_S\boldsymbol{\Phi}_S\boldsymbol{g}_E|^2}{N_E}\right)$$

where P_S represents the transmit power. $\boldsymbol{h}_S$ represents the channel from the transmitter to the RIS. $\boldsymbol{\Phi}_S$ represents the reflection coefficients of the RIS. $\boldsymbol{g}_E$ and $\boldsymbol{g}_S$ represent the channels from the RIS to the eavesdropper and the legitimate receiver. The system bandwidth is B, while the noise powers of the eavesdropper and the legitimate receiver are N_E and N_S. The secrecy rate of the receiver, which can be calculated as $[C_S - C_E]^+$, can be used to evaluate the security level of the RIS link at the physical layer.

6.7.3   Destructive beamforming

In addition to the unwanted signal reradiation, an RIS is capable of reducing the power of the desired signal. This effect can be considered as a destructive beamforming capability of RIS. Destructive beamforming effect could happen as a result of RIS misconfiguration, as an outcome of malicious RIS control, or as a desired property of radio signal suppression in some specific use cases.

Under the assumptions of perfect knowledge of the channel from the transmitter to RIS and from the RIS to the receiver by the RIS controller, the potential of destructive beamforming can be quantified by means of an upper-bound. Consider a system with a single-antenna Tx, a single-antenna Rx, and a RIS consisting of N reflecting elements. The analysis is valid for both UL and DL links. In addition, instead of a single-antenna one can consider a single antenna port at both Tx and Rx. The malicious impact is estimated at a particular sub-band. If the channel is frequency selective, the potential destructive effect is smaller than the derived upper bound (i.e. the provided bound is not tight).

Let $h^d \in \mathbb{C}$ be the component of Tx-to-Rx channel that avoids controllable RIS, $h_k^r \in \mathbb{C}$ be the channel coefficient from Tx to k-th reflective element of RIS, $g_k \in \mathbb{C}$ be the channel coefficient from k-th reflective element of RIS to Rx, $\Theta_k \in \mathbb{C}$ be the phase shift coefficient of k-th reflective element of RIS. At the considered sub-band), the signal is:

$$y = \left(h_d + \sum_k h_k^r \Theta_k g_k \right) s + n$$

The channel gain is:

$$P(\Theta) = \left| h_d + \sum_k h_k^r \Theta_k g_k \right|^2$$

Under these assumptions, the destructive passive beamforming problem for RIS is:

$$\left| h_d + \sum_k h_k^r \Theta_k g_k \right|^2 \to \min_{\Theta}$$

A is the effective area of a single reflection coefficient of RIS, λ is the wavelength, C_k is the coefficient that corresponds to the radiation antenna gain of Tx in the direction of k-th RIS element, the reception gain of Rx from the direction from of k-th RIS element, and the Rx effective area, d_k^{Tx-RIS} is the distance from Tx to the k-th element of RIS, d_k^{RIS-Rx} is the distance from the k-th element of RIS to Rx, $d_{min}^{Tx-RIS} := \min_k d_k^{Tx-RIS}$, $d_{min}^{RIS-Rx} := \min_k d_k^{RIS-Rx}$, $C_{max}^{RIS} := \max_k C_k$, d^{Tx-Rx} is the average length of the propagation path from Tx to Rx, C^{Tx-Rx} is the coefficient that corresponds the radiation antenna gain of Tx in the direction of Rx, the reception gain of Rx from the direction from the k-th RIS element, and the Rx effective area.

Then the following bound holds:

$$\frac{P(\Theta_{min})}{P_{noRIS}} \geq 1 - \frac{2NA}{\lambda} \frac{C_{max}^{RIS}}{C^{Tx-Rx}} \frac{d^{Tx-Rx}}{d_{min}^{Tx-RIS} d_{min}^{RIS-Rx}}$$

It is worth noting that the provided bound is not practically achievable, since it requires perfect knowledge at the RIS controller side about the Rx to RIS channel and Tx to RIS channel. In the case of no adaptive beamforming and close location of the RIS and the receiver the following bound holds:

$$\frac{P(\Theta_{min})}{P_{noRIS}} \geq 1 - \frac{2NA}{\lambda d_{min}^{Tx-RIS}}$$

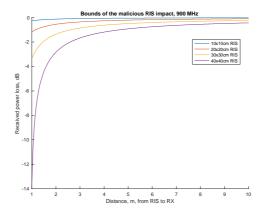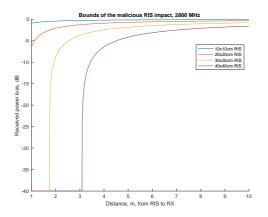Some illustrative results are given in Figure 13 and Figure 14.

Figure 13: Destructive beamforming upper bounds, 0,9 GHz band

Figure 14: Destructive beamforming upper bounds, 2,8 GHz band

6.7.4   Modeling CSI mismatch due to interference and unwanted reradiation

6.7.4.1   CSI mismatch due to interference (In-Band Reradiation)

In wireless networks without RIS, the CSI mismatch due to Discontinuously Time-Varying interference already exists. In this clause the contribution of RIS to the CSI mismatch is defined.
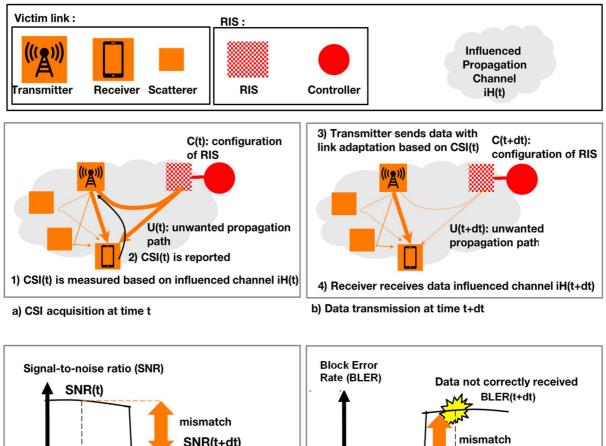
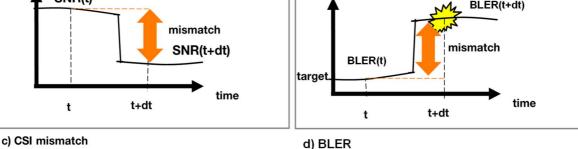### 6.7.4.2   CSI mismatch due to Unwanted reradiations

In this clause, a method to model the impact of unwanted reradiations (Unexpected/Irregular/Discontinuously Time-Varying Out-Of-Band Reradiation) on the closed loop link adaptation is presented.

In this general context, the link adaptation concept is included in any adaptation scheme based on Channel State Information (CSI): adaptive beamforming, adaptive modulation and coding, etc.

As illustrated in the example of Figure 15, a victim link between a transmitter and a receiver is considered, in the presence of an aggressor RIS controlled by a controller.

Figure 15: Modeling Channel State Information mismatch due to time-varying unwanted reradiations

In this clause, a model taking into account the time-variations of the influenced propagation channel of the victim link (the channel being under the influence of the unwanted RIS) over the closed loop link adaptation is described. The time-variation of an unwanted path - i.e. a path reradiated by a RIS and potentially by scatterers- is impacted by the continuous time-variation of the scatterers and the discrete time-variation of the state of the RIS. Hence, the time-variation of an unwanted path is different from the time-variation of a 'normal' propagation path - i.e. a path not reflected by any RIS - and it breaks the continuity of the overall channel time-variation.

More precisely, as illustrated in Figure 15 (see sub-figure a)), at time t, the receiver estimates the current CSI CSI(t) where:

- CSI(t) is a function of the current influenced channel iH(t).

- iH(t) includes the unwanted propagation path(s) U(t) between the transmitter and the receiver (passing by the RIS).

- U(t) is a function of C(t).

- C(t) is the configuration of the unwanted RIS.

The scheduler and the link adaptation scheme at the transmitter side, selects the beamforming, the modulation and coding scheme, etc., based on CSI(t). The transmitter predicts the expected performance, for instance, in terms of Signal-to-Noise Ratio (SNR) and Block Error Rate (BLER). It is denoted SNR(t) as the expected SNR, and BLER(t), as the expected BLER, based on CSI(t) and the link adaptation. SNR(t) and BLER(t), are illustrated in Figure 15 (sub-figures c) and d), respectively).

Then, as illustrated in Figure 15 (sub-figure b)), at time t+dt, the receiver receives data with a link adaptation (an adapted beamforming, an adapted modulation and coding scheme, etc.) based on CSI(t), through the new influenced channel iH(t+dt), where:
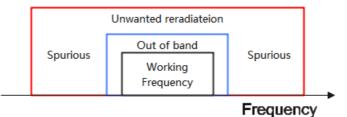
- iH(t+dt) includes the unwanted propagation path(s) U(t+dt) between the transmitter and the receiver (passing by the RIS).

- U(t+dt) is a function of C(t+dt).

- C(t+dt) is the configuration of the unwanted RIS, and the configuration C(t+dt) is different from C(t).

The receiver receives data with the actual SNR SNR(t+dt) that depends on both CSI(t) and iH(t+dt) and an actual BLER BLER(t+dt), illustrated in Figure 15 (sub-figures c) and d), respectively).

As illustrated in in Figure 15 (sub-figures a) and b), respectively), it may happen that U(t+dt) strongly differs from U(t), and that iH(t+dt) strongly differs from iH(t). In some cases, this may lead, as illustrated in sub-figure c) to a strong degradation from SNR(t) to SNR(t+dt), i.e. a strong negative CSI mismatch. As a consequence, as illustrated in sub-figure d), the BLER(t+dt) can be much worse than the expected value BLER(t).

6.7.5   Spurious reradiation

The unwanted reradiation of RIS consists of spurious reradiation and out-of-band reradiation, where out-of-band reradiation is illustrated in Figure 16.

Figure 16: Relationship between spurious and out-of-band domain

The spurious reradiation is the emission on frequencies, which are outside the necessary bandwidth and the level of which may be reduced without affecting the corresponding transmission of information. The relationship between spurious reradiation and out-of-band reradiation is shown in the figure. Ideally, the frequency of both the impinging wave and reflected wave should be contained in the range of working frequency.

Spurious reradiation include harmonic reradiation, parasitic reradiation, intermodulation products and frequency conversion products, as specified in Recommendation ITU-R SM.329 [i.3]. Normally, the spurious reradiation (not including multi-mode reradiation described in clause 7.6 of the present document) for passive RIS is very small and can be neglect. However active RIS would suffer more serious spurious problem than passive RIS. This is because some active components like amplifier or modulator may exist in active RIS and such components will bring more spurious reradiation.

When RIS is working surrounded by other electric products, the spurious reradiation might introduce performance degradation to other equipment's. In order to restrict the spurious reradiation, Radiated Spurious Emission (RSE) as a RF and EMC test needs to be implemented. The width of test domain depends on the RIS's working frequency. One example can be the test range for FR1, which is from 30 MHz up to 5th harmonic of the upper frequency edge of the operating band in GHz. While, for FR2 the test range is from 30 MHz up to 2nd harmonic of the upper frequency edge of the operating band.

6.8   Polarized RIS element modeling

Nowadays almost all NR devices support dual polarization as a basic and mandatory feature, specified by 3GPP. For example, legacy NR port-selection codebook supports dual polarization. Similarly, RIS antenna elements can also support dual polarization like dual polarized antennas, wherein, the phase-shifts provided by RIS element may be controlled by varying the vertical and horizontal state of polarizations. In other words, as an example the dual-polarized RIS may control the amplitude or phase-shifts of the reflected Electromagnetic (EM) waves in two orthogonal polarizations as shown in Figure 17.
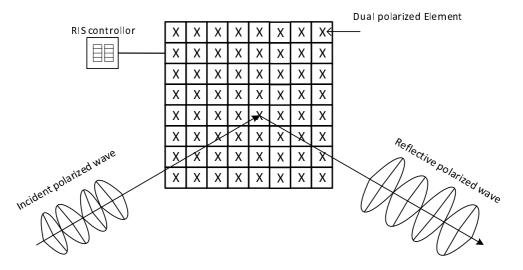

Figure 17: Dual polarized RIS

The polarization of the RIS antenna elements can be extended to multi-polarizations. To achieve the best communication performance, the design of the RIS communication channel models need to consider the effect of polarization at RIS antenna elements in addition to the polarization at transmitter and receiver antennas, as currently supported by legacy NR.

If RIS supports dual polarization capability (e.g. dual-polarized RIS), then the signal model at a RIS element can be expressed as:

$$\mathbf{y} = \mathbf{H}_\mathrm{p}\mathbf{x},$$

where $\mathbf{x}$ and $\mathbf{y}$ are the input and output polarized signals at a RIS element, and the polarization channel matrix $\mathbf{H}_\mathrm{P}$ has the form:

$$\mathbf{H}_\mathrm{P} = \begin{bmatrix} \beta^{VH}e^{-j\phi^{VV}} & \beta^{HV}e^{-j\phi^{HV}} \\ \beta^{VH}e^{-j\phi^{VH}} & \beta^{HH}e^{-j\phi^{HH}} \end{bmatrix},$$

where $\phi^{pq} \in [0, 2\pi]$ and $\beta^{pq} \in [0, 1]$ denotes the phase and amplitude of reflection induced by the RIS element from polarization p to polarization q with $p, q \in \{V, H\}$ vertical and horizontal polarization.

If an RIS can tune the RIS reflecting phase and amplitude in each component of the polarization channel matrix $\mathbf{H}_\mathrm{P}$, then it is possible to convert an impinging polarized signal into a desired polarized signal.

7   Channel Estimation
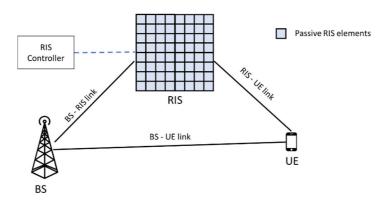
7.1   Reference scenarios

7.1.1   General description

Three case studies are analysed:

- RIS cannot perform on-board channel estimation.

- RIS can perform on-board channel estimation.

- The direct link is present.

7.1.2   RIS cannot perform on-board channel estimation

In this scenario, it is considered that the RIS utilized in the communication is unable to perform onboard channel estimation. This can happen when the RIS is equipped with all passive elements, as shown in Figure 18, that can apply configurable phase shifts to the impinging signals or can provide a certain degree amplification.

Figure 18: RIS-aided communication scenario where RIS is equipped with all passive elements

In this case, it is assumed that the RIS does not consist of any RF chain or cannot perform any local baseband processing to support the onboard channel estimation. The channel estimation can only be performed at the BS/UE by utilizing RIS-aided link.

7.1.3   RIS can perform on-board channel estimation

Along with the passive elements, the RIS can be equipped with a few active elements as shown in Figure 19, that can facilitate active reception/transmission and local baseband processing.
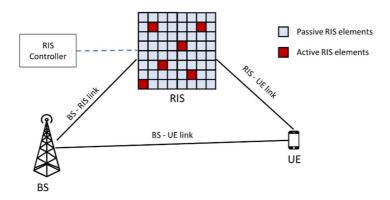
Figure 19: RIS-aided communication scenario where RIS is equipped with a few active elements

The placement of the active elements can be fixed or flexible with sperate RF chains associated with each active element or a single RF chain shared by multiple active elements. Using these active elements, an RIS can perform on-board channel estimation task. The power requirement will increase due to the introduction of active elements, however higher gain channel estimates can be obtained at RIS due to the reduced path loss as compared to the overall BS-RIS-UE link. Channel estimation methods that build on this framework can be utilized for obtaining separated channel estimates between BS-RIS and RIS-UE links as well.

7.1.4   Availability of direct link between gNB and UE

The methods for channel estimation in an RIS-aided communication can vary based on the availability of the direct path between the BS-UE. Based on this, two scenarios can be considered as shown in Figure 20.
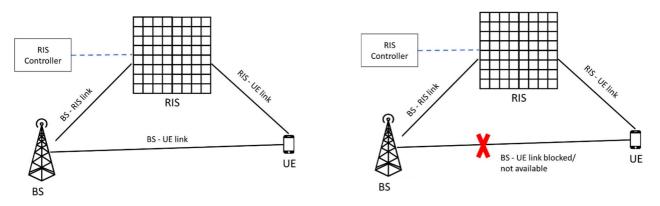

Figure 20: Scenarios for RIS-aided channel estimation based on the availability of the direct link between BS-UE

In the first scenario, depicted in the left figure, a direct link between the BS-UE is available along with the reflected link via the RIS i.e. BS-RIS-UE link. In this scenario, the channel estimation at the UE (in the case of downlink transmission) or at the BS (in the case of uplink transmission) can utilize methods that takes into consideration both the available communication links viz., BS-UE and BS-RIS-UE. Whereas, in the second scenario, shown in the right figure, the direct link between the BS-UE is not available i.e. the direct link is obstructed completely due to blockage, direct link is a weak communication link due to highly fading propagation environment and cannot be utilized, etc. The channel estimation methods which can be utilized in this scenario are likely not to rely upon the availability of the direct link and hence developed only upon the availability of reflected path between BS and UE i.e. BS-RIS-UE link.

7.2   Cascaded and separated channel estimation

7.2.1   General description

In the present clause, channel estimation methods are described that belong to two different categories:

- Methods to estimate the end-to-end channel.

- Methods to estimate the individual channels.

7.2.2   Methods to estimate the end-to-end cascaded channel

7.2.2.0   General

In an RIS-aided communication system, apart from the direct link, there exists an additional communication link between the BS/TRP and the UE which is via the RIS. Cascaded channel estimation technique estimates the end-to-end effective channel gains through the RIS-aided link and inherently capture the effect of the phase shifts provided by the RIS elements. Three different methods to estimate the cascaded channels using the RIS-aided link are described in the clauses as follows.
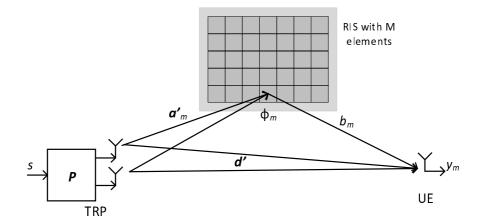
7.2.2.1   Element-wise RIS channel estimation

7.2.2.1.0   General

First, an exemplary system model including one RIS element is presented. Secondly, an exemplary system model including all RIS elements of a single RIS is presented. Downlink (DL) models are discussed here, but the same or similar models may be applicable to the Uplink (UL). For simplicity, consider a single-antenna UE and a narrowband system, i.e. a subcarrier of an OFDM system. Such a model may also cover the case with a multi-antenna UE that combines multiple received signals into a single received signal by using receiver processing, i.e. digital or hybrid beamforming or combining techniques.

7.2.2.1.1   System model including one RIS element

An exemplary scenario is illustrated in Figure 21.

Figure 21: System model for element wise RIS channel estimation

The equivalent received complex-valued scalar signal y_m at the UE is given by:

$$y_m = (b_m \boldsymbol{a'_m} \phi_m + \boldsymbol{d'})\boldsymbol{P}s + z = (\boldsymbol{c'_m}\phi_m + \boldsymbol{d'})\boldsymbol{P}s + z$$

wherein:

- s is the complex-valued scalar symbol, i.e. a known Reference Signal (RS) or pilot symbol.

- $\boldsymbol{P}$ is the complex-valued precoding vector of dimension $N_T \times 1$, where N_T is the number of transmit antennas or antenna ports, i.e. at a network-side TRP.

- $\boldsymbol{d'} = [d'_0 \quad \cdots \quad d'_{N_T-1}]$ is the complex-valued channel between the TRP and the UE, excluding propagation paths via the RIS, of dimension $1 \times N_T$.

- $\boldsymbol{a'_m}$ is the complex-valued vector channel between the TRP and the RIS element, of dimension $1 \times N_T$.

- $\boldsymbol{c'_m} = b_m \boldsymbol{a'_m}$ is the cascaded complex-valued vector channel between the TRP, RIS element m, and the UE, of dimension $1 \times N_T$.

- ϕ_m is the complex-valued scalar RIS element factor of RIS element m, with m=1, …, M. In a passive RIS, the factor may have a fixed amplitude, i.e. a unit amplitude ($|\phi_m| = 1$). In an active or hybrid RIS, the amplitude may be variable and controllable. In some cases, i.e. even for a passive RIS, an RIS element may be turned off, i.e. $\phi_m = 0$ or $\phi_m \approx 0$. A RIS element may be in a certain state (ϕ_m) at a time and is assumed to be applicable to all sub-carriers within a certain bandwidth.

- b_m is the complex-valued scalar channel between the RIS element and the UE.

- z is the additive noise and interference.

The model can be further simplified by including the TRP precoding $\boldsymbol{P}$ into the TRP-to-RIS channel:

$$y_m = (b_m a_m \phi_m + d)s + z = (c_m \phi_m + d)s + z$$

wherein:

- $d = \boldsymbol{d}' \boldsymbol{P}$ is the complex valued scalar effective direct TRP-to-RIS channel (including TRP precoding).

- $a_m = \boldsymbol{a}_m' \boldsymbol{P}$ is the complex-valued scalar channel between the TRP and the RIS element.

- $c_m = b_m a_m$ is the cascaded complex-valued scalar channel TRP to m:th RIS element to UE.

7.2.2.1.2 System model including all RIS elements

An exemplary model including all RIS elements can be obtained by adding the signals corresponding to all *M* RIS elements of the RIS ($c_m \phi_m s$):

$$y = \big((\boldsymbol{a}\odot\boldsymbol{b})\boldsymbol{\Phi} + d\big)s + z = (\mathbf{c}\boldsymbol{\Phi} + d)s + z$$

wherein:

- $\boldsymbol{a}$ is the complex-valued vector channel between the TRP and the RIS, of dimension $1 \times M$, where *M* is the number of RIS elements.

- $\boldsymbol{b}$ is the complex-valued vector channel between the RIS element and the UE, also $1 \times M$.

- $\boldsymbol{c} = \boldsymbol{a}\odot\boldsymbol{b} = \boldsymbol{b}\odot\boldsymbol{a}$ is the element-wise vector product of $\boldsymbol{a}$ and $\boldsymbol{b}$.

- $\boldsymbol{\Phi}$ is the complex-valued vector of dimension $M \times 1$ containing the *M* RIS element factors ϕ_m. $\boldsymbol{\Phi}$ may correspond to the RIS state.

In the case of rectangular RIS, let M_x denote the number of RIS elements in a first direction, i.e. horizontal, and M_y denote the number of RIS elements in a second direction, i.e. vertical, for instance such that $M=M_x*M_y$. Using the element-wise RIS channel estimation method, the cascaded channel gains can be estimated at the UE by individually capturing the effect of the phase-shifts contributed by each RIS element. Thus, in the communication system, wherein the BS/TRP is communicating with a UE with the help of an RIS consisting of M RIS elements as shown in Figure 22, the overall channel estimate for the cascaded link (BS-RIS-UE) can be the computed as an effective gain obtained by all the M-RIS elements.
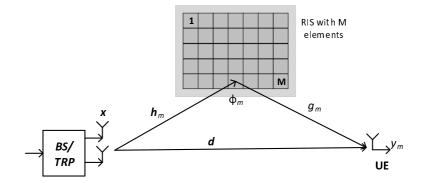

Figure 22: System model for element wise RIS channel estimation

The element-wise channel estimation method may benefit from highly efficient channel estimation due to the consideration of phase-shifts from each RIS element. However, in the case of large RIS surfaces, the large number of RIS elements may introduce undesired latencies and pilot/reference signal overhead reflected by each RIS element.

7.2.2.1.3   Sub-surface based RIS channel estimation

To overcome the latency and pilot overhead in the element-wise channel estimation method, the complete M-element RIS surface can be divided into S sub-surfaces, each constituting a group of RIS elements. Then the channel estimation can be performed at the sub-surface level instead of an element-wise estimation. Consider a similar communication system wherein a BS/TRP communicates with a UE via an M-element RIS. Let the total number of RIS elements be divided into S sub-surfaces as shown in Figure 23.

Figure 23: System model for sub-surface based RIS channel estimation

Then, the overall channel estimate at the UE will be the effective channel reflected by each of these sub-surfaces constituting the RIS-reflected cascaded channel.

7.2.2.2   Configuration-wise RIS channel estimation

To further reduce the latency and pilot overhead in the sub-surface based channel estimation method a codebook approach can be used. The RIS can be configured with a number of pre-defined configurations. The pre-defined configurations can, for example, refer to multiple beams in different directions as shown in Figure 24.
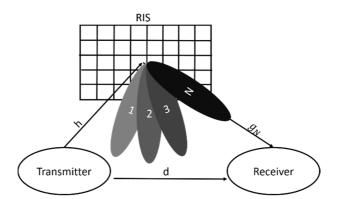

Figure 24: System model for configuration-wise RIS channel estimation

Then, the channel estimation can be performed at the RIS level sequentially for each of the pre-defined configurations. This method can be especially interesting in the sub-6 GHz band, where the number of RIS elements is small and the achieved beam directivity is limited. Hence, the required coverage area can be covered with a small number of pre-configured beams.

7.2.2.3   Single RF chain enabled RIS channel estimation

The nearly passive RIS-assisted wireless communication requires lengthy training periods to estimate the channel. To shorten the training time, a single active Radio Frequency (RF) chain for baseband reception can be connected to the output of RIS illustrated in Figure 25.
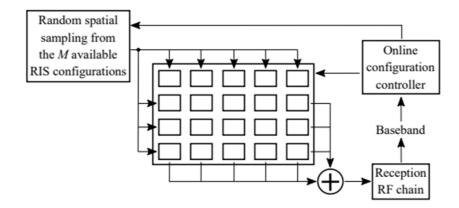
**Figure 25: Block diagram of the proposed RIS hardware architecture including a
single active reception RF chain for explicit channel estimation at the RIS side**

This single RF chain enabling baseband channel estimation via pilot signals consists of a low noise amplifier, a mixer down converting the signal from RF to baseband, and an analog to digital converter. In this way, the accurate channel estimation can be conducted at the RIS and the training time can be shortened with specifically designed algorithm.

7.2.3   Methods to estimate the separated/individual RIS channels

The cascaded channel path (BS-RIS-UE) in the RIS-aided communication consists of two individual paths namely, the BS-RIS path and the RIS-UE path. The estimation of individual RIS channels can be defined as obtaining these two paths i.e. BS-RIS and RIS-UE channels separately. Due to the introduction of RIS, individual RIS channels may result in a higher rank channel for at least one of the individual channels as compared to the end-to-end cascaded channels. Furthermore, due to the high-resolution channel gains, estimating the individual RIS channels may provide enhanced performance in terms of higher signal-to-noise-ratio, throughput, BLER, data rates, etc. Especially in scenarios wherein the RIS and either the BS/UE are static, and only the UE/BS are moving, acquisition of the individual separated channels is critical to analyse the impact of the individual channels. The methods for separated channel estimation depend on different type of RIS. In the case of passive RIS, the channel estimation cannot be performed at the RIS node and can only be either done at the BS or UE. In such a case, estimating individual separated channels may be performed using different techniques. These include:

a)   Decomposition of the end-end cascaded links into separated individual channel estimation, by using signal processing tools such as eigen vector decomposition, matching pursuit using sparse signal processing, etc. This can be done at the UE node in the case of downlink transmission or at the BS in case of the UL transmission.

b)   Anchor nodes can be deployed (i.e. by the BS network), for the task of channel estimation that may be closely located to the RIS surfaces. Such anchor nodes can be useful for estimating the RIS-aided channels. Finally, in the case of a semi-active or active RIS, the active RIS elements can be configured to be utilized to perform the channel estimation task.

7.3   Estimation methods for unstructured channel models

As for unstructured channel models, various channel estimation methods exist [i.15]:

- Least Squares (LSs) Estimators, including on-off schemes, discrete Fourier transform methods, methods based on the Hadamard matrix for the single-user case, as well as the direct channel estimation method and schemes that exploit the common RIS-BS channel for the multi-user case.

- Linear Minimum Mean-Squared-Error methods.

Other methods include the following:

- Differential Data-Aided Beam Training. the beam training based on codebook selection requires the transmission of some reference signals to test the different phase configurations of the codebook. Relying on data transmission and reception based on differential modulated non-Coherent Demodulation Schemes (non-CDS), zero overhead beam training for RIS can be achieved. This method contains two stages. In the first stage, beam training is executed, and at the same time, non-coherent transmission is performed over the BS-UE direct link. In the second stage, the best phase configuration is loaded to the RIS and non-coherent data symbols are transmitted over the enhanced reflective BS-UE link via RIS. At the BS, the received differential data can also be used for the determination of the best beam for the RIS. Therefore, the efficiency of the system is significantly enhanced since reference signals are fully avoided. After choosing the best codebook, NCDS is still more suitable to transmit information for high mobility scenarios as compared to the classical CDS.

- Low-to-zero overhead channel estimation for mobile users: requiring knowledge of full CSI of the RIS will lead to some acquisition overhead. Optimizing the RIS for illumination of the area centered around the Mobile User (MU) will reduce the overhead. First, the position of the MU is to be estimated. Then, the RIS phase-shift is designed to illuminate around the location of the MU. Finally, the end-to-end channel estimation is conducted by using standard (i.e. least squares) channel estimation techniques.

7.4   Methods for structured channel models

As for structured channel models, various channel estimation methods exist [i.15]:

- Single-user case: one-stage channel estimation methods, two-stage channel estimation methods, beam training methods.

- Multi-user case: double-sparse based channel estimation, and methods based on exploiting the common RIS-BS channel methods.

7.5   Methods based on availability of channel state information

The transmission design of RIS-aided systems highly relies upon the availability of CSI, which in turns determines how often channel estimation is performed and hence the corresponding channel estimation overhead. Based on the availability of CSI RIS-aided communication systems can be classified into three categories [i.15]:

- Systems designs based on instantaneous CSI.

- Systems designs based on the so-called two-timescale CSI.

- Systems designs that rely on fully long-term CSI.

For the case of systems designs based on instantaneous CSI, the overall CSI of the system is assumed to be available at the BS. The RIS-related channels can be the cascaded channels or the individual channels depending on the channel estimation method being used. In this case, these channels need to be estimated at each channel coherence block. Therefore, the number of time slots required for channel training is often proportional to the number of reflecting elements, i.e. for unstructured channel models.

To overcome the overhead of methods based on instantaneous CSI, the two-timescale beamforming design can be utilized. The main idea is that the active beamforming vectors at the BS are designed based on the instantaneous effective/aggregated BS-user channels that are the superposition of the direct and RIS-reflected channels, while the phase shifts at the RIS are designed based on long-term CSI, such as their distribution parameters including channel mean and channel covariance matrices. In each coherence block, only the instantaneous effective channel of each user needs to be estimated and the channel training overhead is equal to the number of users, which is the same as for legacy systems without RIS. Furthermore, since the long-term CSI remains usually invariant for a large number of channel coherence blocks, the phase shifts of the RIS can be updated at a much lower rate than the fast fading fluctuations, which significantly reduces the computational burden and feedback overhead.

In the two-timescale design, the instantaneous effective CSI needs to be estimated in each coherence block. To further reduce the channel estimation overhead, a possible approach is based on transmission designs that require only long-term CSI. Specifically, at the beginning of the transmission, the BS estimates or measures the long-term CSI, based on which the BS computes the beamforming vector and the phase shifts that are used in all the subsequent coherence blocks until the long-term CSI changes. This reduces significantly the channel estimation overhead at the cost of some performance degradation that depends on the characteristics of the channel.

7.6   Hybrid RIS-assisted channel estimation

RIS comprising passive elements can only act as adjustable reflectors. Hybrid RIS cannot solely reflect the impinging waveform in a controllable fashion, but are also capable of sensing and processing a portion of it via some active reception elements. A hybrid RIS comprises hybrid metasurface elements which can simultaneously reflect a portion of the impinging signal and receive a portion of it in a controllable manner. Suppose a hybrid metasurface comprises several meta-atom elements, which are connected to a digital controller via multiple receive RF chains, the observed signals except the reflected is locally processed, via analog combining and digital processing. Channel estimation can be done at the hybrid RIS side by processing these received signals which will shorten the training time.
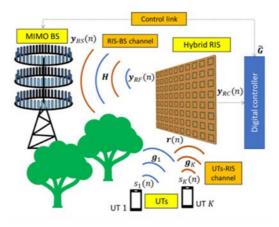

Figure 26: Example of hybrid RIS-empowered uplink multi-user MIMO system

8   Key performance indicators and evaluation methodology

8.1   Key performance indicators

8.1.1   Rate/Throughput

Throughput is considered from the user and system perspectives. From a user perspective, user throughput is defined as the number of correctly received bits, i.e. the number of bits contained in the SDUs delivered to Layer 3, averaged over a certain period of time. In an RIS-assisted system, the correctly received bits can be directly from BS/user for DL/UL cases, or from RIS, or a combination of them. In the case the total bandwidth is aggregated across multiple bands (one or more TRxP layers), the user throughput is summed over the bands. From a system perspective, system throughput is the aggregate throughput of all users.

8.1.2   Spectral Efficiency

Spectral efficiency is the aggregate throughput of all users divided by the channel bandwidth of a specific band divided by the number of TRxPs and is measured in bit/s/Hz/TRxP. The channel bandwidth for this purpose is defined as the effective bandwidth multiplied by the frequency reuse factor, where the effective bandwidth is the operating bandwidth normalized appropriately considering the uplink/downlink ratio.

8.1.3   Coverage (User Percentiles)

Coverage is defined as the area where more than X % of the users can achieve a user throughput of R. For instance, coverage is often defined as the area with more than 95 % of the users whose throughputs are higher than 1 Mbps.

8.1.4   Energy Efficiency

Network energy efficiency is the capability of an RIS-assisted system to minimize the radio access network energy consumption in relation to the traffic capacity provided. Device energy efficiency is the capability of an RIS-assisted system to minimize the power consumed by the device modem in relation to the traffic characteristics. RIS energy efficiency is a measure of the RIS energy consumption in relation to assisting the traffic delivery from the transmitter to the receiver.

The energy efficiency of the network, the device, and the RIS can relate to the support for the following two aspects:

- Efficient data transmission in a loaded case. Efficient data transmission in a loaded case is characterized by the spectral efficiency defined above.

- Low energy consumption when there is no data. Low energy consumption when there is no data can be estimated by the sleep ratio. The sleep ratio is the fraction of unoccupied time resources (for the network) or sleeping time (for the device or RIS) in a period of time corresponding to the cycle of the control signalling (for the network) or the cycle of discontinuous reception (for the device or RIS) when no user data transfer takes place.

8.1.5   Security

Secrecy rate plays an important role in physical layer security. It is a metric that defines the rate at which the transmitted signal reaches the legitimate receiver without any form of invasion from the eavesdropper. One definition of the secrecy rate is the non-negative difference between the capacity of the intended receiver and that of the eavesdropper. Without the precise knowledge of eavesdropper's identity and channel, the secrecy rate for each receiver can be estimated by treating all legitimate but unintended terminals in a network as potential eavesdroppers

8.1.6   Latency

To evaluate RIS-assisted systems, latency can be defined from two perspectives: user plane latency and RIS control plane latency. User plane latency is the contribution of the radio network to the time from when the source sends a packet to when the destination receives it (in millisecond). It is defined as the one-way time it takes to successfully deliver an application layer packet/message from the radio protocol layer 2/3 SDU ingress point to the radio protocol layer 2/3 SDU egress point of the radio interface for a given service in unloaded conditions, assuming the UE is in the active station. In RIS-assisted systems, user plane latency is defined as end-to-end latency, i.e. from BS to user in DL cases and from user to BS in UL cases. RIS control plane latency is the time duration to (re-)select and (re-)configure RIS, which can be evaluated for different RIS control plane protocols.

8.1.7   Reliability

Reliability relates to the capability of transmitting a given amount of traffic within a predetermined time duration with high success probability. Reliability is the success probability of transmitting a layer 2/3 packet within a required maximum time, which is the time it takes to deliver a small data packet from the radio protocol layer 2/3 SDU ingress point to the radio protocol layer 2/3 SDU egress point of the radio interface at a certain channel quality.

8.1.8   Overhead

In general, overhead refers to signalling between BSs and users that enable the transmissions rather than directly contain the traffic data. In RIS-assisted systems, overhead also includes the signalling to (re)select, enable, (re-)configure, and control RIS.

8.2   Design Parameters

8.2.1   RIS size

The size of RIS panel needs to be sufficiently large so that the re-radiated signal power meets requirements. One potential requirement of an RIS link is to provide comparable signal strength to unblocked LOS link, which is necessary in multiple use cases (i.e. avoid blockage/penetration loss, provide additional spatial multiplexing rank, etc.). Based on the far-field free space path loss model introduced in the present document, the RIS size requirement can be derived. Given a BS-RIS-UE link, the LOS distance between the BS and UE is represented by d_{LOS}. The BS and UE antenna gains for the LOS path are G_t^{LOS} and G_r^{LOS}, which can be different from G_t and G_r for the RIS-aided link. The LOS path loss is then:

$$PL_{LOS} = \frac{16\pi^2 d_{LOS}^2}{G_t^{LOS} G_r^{LOS} \lambda^2}$$

If the path loss of the RIS-aided link needs to be smaller than or equal to PL_{LOS}, the requirement on the RIS area is:

$$MN d_x d_y \geq \frac{d_t d_r \lambda}{d_{LOS}} \sqrt{\frac{G_t^{LOS} G_r^{LOS}}{G_t G_r F(\theta_t, \phi_t) F(\theta_r, \phi_r) A^2}}$$

where d_x and d_y represent the width and length of each RIS element, and the RIS is assumed to have $M \times N$ elements in total. d_t and d_r represent the distance between the transmitter/receiver and the center of RIS. $F(\theta_t, \phi_t)$ is the normalized radiation pattern of each RIS element to the transmitter, in which θ_t and ϕ_t represent the elevation angle and azimuth angle from the center of the RIS to the transmitter. Similarly, $F(\theta_r, \phi_r)$ represent the normalized radiation pattern to the receiver's direction. The variable A is the amplitude of reflection coefficients of each RIS element, which is assumed to be the same for all the RIS elements.

8.2.2   Electromagnetic Field Exposure

A relevant issue for future wireless networks is the growing concerns for electromagnetic pollution. Although, at present, non-ionizing radio frequency radiations have not been associated to any health condition, the continuous exposure to ElectroMagnetic Fields (EMFs) is a factor that raises concerns among end-users and diminishes their acceptance of emerging transmission technologies and massive network deployments. In general, the EMF requirements are formulated in terms of Specific Absorption Rate (SAR) requirements. Specifically, each portable device complies with specific SAR limits of radiation that are considered safe for the body. The challenge of fulfilling SAR compliance is exacerbated by the use of multiple transmit antennas in portable wireless devices, which increases the exposure for a given total transmit power, due to the combinations of the precoding gains and phases across the antennas. In this context, RIS need to be considered in the evaluation of fulfilling SAR compliance and can be utilized to reduce the EMF at the mobile terminals.

8.2.3   Carrier Frequency

Carrier frequency is the center frequency on which RIS control channel and data channel operate. The control information can be signalled to RIS on a different frequency than the channels/signals to be reflected.

8.2.4   Bandwidth

Bandwidth is the maximum aggregated system bandwidth. The bandwidth may be supported by single or multiple radio frequency carriers.

8.3   Reference scenarios for evaluation

The performance improvement to communication networks brought by RIS needs to be comprehensively evaluated. In addition to the example scenario in which RIS is deployed on the walls of an indoor office defined in ETSI TR 138 901 [i.2], the network performance in the following applications of RIS (defined both for indoor and outdoor scenarios) can be evaluated.

Figure 27 demonstrates the most common and intuitive application of RIS, i.e. serving as a solution to blockage issues, which applies to both outdoor and indoor scenarios.
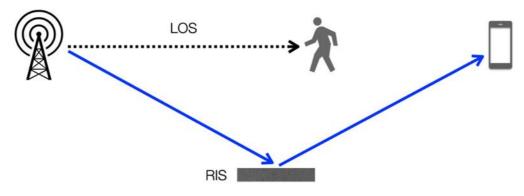
Figure 27: RIS as a solution to blockage

Figure 28 illustrates a variant of the blockage problem shown in Figure 27, in which the BS deployed in one corridor needs to serve UEs in a perpendicular hallway.
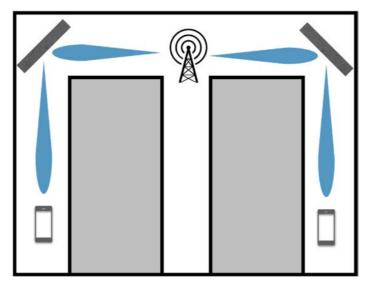

Figure 28: RIS redirects beams to form link between BS and UE in different hallways

Due to the high penetration loss, such a link is not feasible without the assistance of RIS. More BSs need to be deployed at the intersections of corridors to achieve the full coverage without RIS. In the figure, for example, at least 3 BSs are needed to cover all corridors without RIS, whereas 1 BS is enough to achieve full coverage with the assistance of RIS. This deployment can be quite common in real-world scenarios. The system-level simulation of this scenario can be developed based on the indoor-office and indoor-factory scenario in ETSI TR 138 901 [i.2].

Figure 29 shows another potential scenario in which RIS can help to avoid blockage. By utilizing multiple RIS in a cascading manner, a link can detour around multiple blockers without incurring extra delays.

Figure 29: Cascading RIS links assist UEs to form links with BSs regardless of blockage

Similarly, the system-level simulation of this scenario can be developed based on the indoor-office and indoor-factory scenario in ETSI TR 138 901 [i.2].

Figure 30 shows an outdoor scenario, in which a BS on the roof of a building serves UE in street canyon using a huge RIS installed on the wall of the opposite building.
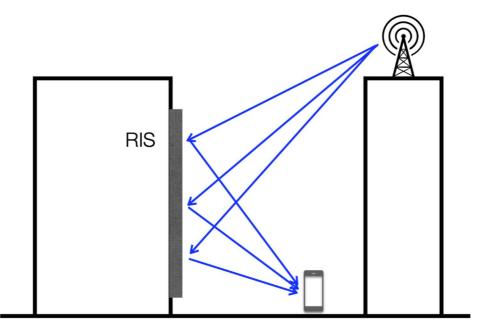

Figure 30: BS serves UE in street canyon using large RIS on building walls

The size of RIS can be very large, which means that the traditional plane wave model may not be valid anymore and a spherical wave model is required. This scenario can be defined based on the urban macro/micro scenarios introduced in ETSI TR 138 901 [i.2].

Figure 31 shows an example application of RIS in an Outdoor-to-Indoor (O2I) scenario, in which BS can serve UE in underground garage with the help of RIS links, given the extraordinary blockage and O2I loss. The height of UEs in this case also needs to be defined differently. This scenario as well as other O2I scenarios can usually be defined based on the urban macro/micro scenarios described in ETSI TR 138 901 [i.2].
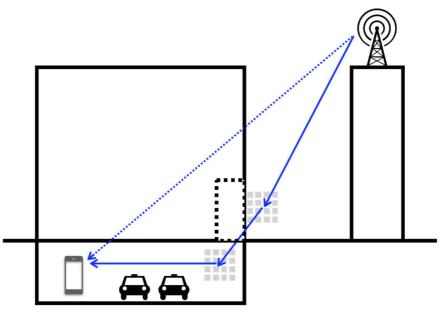
**Figure 31: RIS application in an O2I scenario, in which BS serves UE
in underground garage using RIS**

RIS may improve the network performance in other scenarios without blockage. Figure 32 illustrates the application of RIS to configure the MIMO channel between BS and UE.
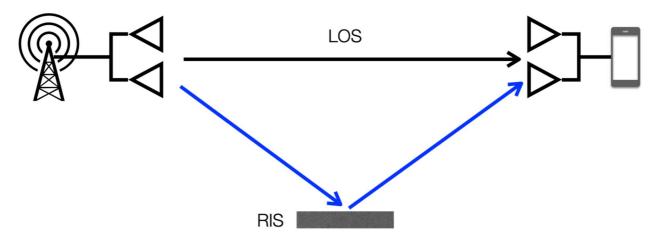

Figure 32: Utilizing RIS with MIMO: multiplexing and interference management

When the BS-UE LOS channel is low-scattering, utilizing RIS can provide extra scattering and channel multiplexing gain to the MIMO system. On the other hand, if the BS is an interferer to the UE, optimizing RIS coefficients can be a strategy to reduce the potential interference. This application is applicable to both outdoor and indoor scenarios. The performance evaluation of such a MIMO system is of great significance, especially when operating on a wide band, since the delay difference between the LOS channel and RIS channel can impair the MIMO beamforming.

An RIS can also be applied for secure communication, as is illustrated in an example scenario in Figure 33. Without RIS, the data sent to a UE can be easily leaked to eavesdroppers via natural reflections by the wall, ceiling, etc. To solve this problem, RIS can redirect the reflections to a "trusted region", which hence reduces the data leakage to potential eavesdroppers and enhances the communication security.
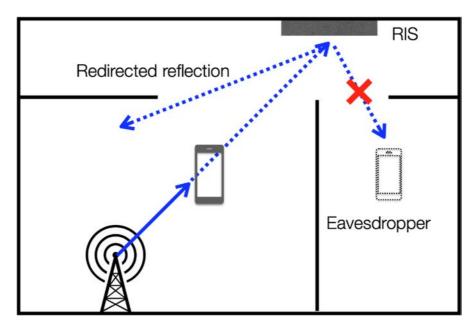
Figure 33: Utilizing RIS for secure communication

As a configurable component that affects the communication channel, an RIS potentially provides a new degree of freedom for multiple access. An example of RIS multiple access is demonstrated in Figure 34, in which different BS-UE links can utilize different sub-arrays on a RIS panel. The feasibility of this multiple access strategy needs to be evaluated in system-level simulators.
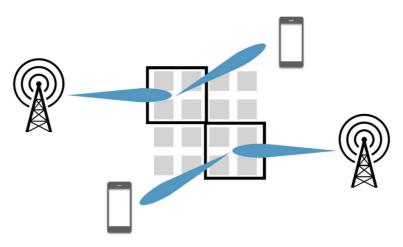

Figure 34: RIS multiple access

8.4 Evaluation methodology

8.4.1 Link-level evaluation

Link-level evaluation is referred to simulate a point-to-point communication link, and evaluates metrics such as bit/block error rate for a given signal to interference and noise ratio. These simulations can be performed based on the channel models, the channel estimation methods, and the transmission methods reported in the present document.

8.4.2 System-level evaluation

System-level simulation is referred to obtain system/network level performance of cellular networks for different deployment configurations (indoors, outdoors, urban/suburban/rural areas, motorways), different frequency bands, and different scheduling policies. System-level simulations provide coverage/capacity metrics such as throughput per square kilometre, throughput per unit of bandwidth, number of users simultaneously supported by the network, and fairness in access to the network.

Basic configurations and parameters for RIS deployment and link are here described for evaluation using system-level simulations, using the models in ETSI TR 138 901 [i.2] as the baseline. The considered parameters are shown in Table 4.

Table 4: Parameters for system-level simulation of RIS-aided communication

Name	Example Value
Horizontal (2D) distribution	Uniform/scenario-specific
Height	Outdoor: Higher than UE and lower than BS, i.e. 2 ~ 10 m Indoor: different height for RIS on the ceiling and wall (i.e. 3 m and 1,5 m, respectively); dependent on the floor
Orientation	Scenario-specific, i.e. RIS on walls has horizontal orientation, and RIS on ceilings will point downwards
Indoor/outdoor distribution	An indoor RIS ratio can be specified for urban scenarios, i.e. 20 %
Min 2D distance to BS/RIS	Dependent on the RIS deployment scenario; Similar values to Min 2D distance of BS-UE link in the corresponding scenario
[Min, Max] 2D distance to UE	Dependent on the RIS deployment scenario, i.e. [1 m, 5 m]
Channel models	Dependent on RIS height. I.e. side link channel model (i.e. the model defined in 3GPP TR 37.885 [i.19]) is more suitable for RIS-UE links if RIS height is closer to urban UE height
Molecular absorption	I.e. HITRAN model for sub-THz
Wave models	Plane wave/spherical wave
RIS size	Dependent on scenarios, i.e. the RIS size can be large
RIS antenna array	Dependent on carrier frequency, i.e. 16 * 16; Sub-array should be supported
RIS antenna element pattern	Similar to BS/UE antenna element configurations (directional/omnidirectional)
Codebook	BS/RIS/UE codebook design
RIS delay in setting RIS beamforming weights	Different values based on RIS deployment scenario

The proposed parameters define deployment, channel, antenna, and beamforming models of RIS. The RIS deployment parameters are generally similar to UE deployment parameters and needs to be scenario-specific (i.e. height and orientation of RIS on the ceiling and wall). Min and Max 2D distances between a RIS and a BS/RIS/UE need to be configured based on the RIS deployment scenario. The channel model of RIS-UE link also depends on the distance and height. If RIS-UE distance is small and RIS height is close to UE height in urban scenarios, a side link channel model may be more applicable compared with the BS-UE channel model. The size of RIS is also an important parameter to consider in system-level simulators.

Using RIS to enhance the coverage when blockage happens is a preferable feature in higher-frequency bands, i.e. the sub-THz band. A comprehensive evaluation of RIS performance hence needs to cover the sub-THz frequency range, while the typical ETSI TR 138 901 [i.2] model is only applicable to frequency up to 100 GHz. This requires a sub-THz RIS channel model to be implemented in system-level simulators, including features like molecular absorption. In this regard, the synergy with the ISG THz is beneficial.

It is important to model the far-field channel and near-field channel separately for RIS-aided links. In the far-field region, the transmitted electromagnetic signal can be approximated with plane waves, and the difference in Rx signal phase at adjacent RIS elements is uniform on the entire array. On the other hand, the spherical wave model is more accurate in the near-field region, in which scenario the phase variance at each RIS element becomes non-linear. However, applying the spherical wave model to a large RIS array with thousands of elements can be computationally complicated, especially in a system-level simulation that involves multiple RIS panels. The trade-off between modeling accuracy and the computational load needs to be considered for near-field channel modeling. One method is to divide any antenna array into sub-arrays, and only consider the spherical wave fronts on the sub-array level. The phase variance of antenna elements in the same sub-array, which forms a smaller aperture, is still modeled with the plane wave model to maintain a manageable computational load. Similar strategies can be applied to RIS modeling in system-level simulator.

In system-level simulators the antenna array model, codebook, and beamforming model of RIS need to be defined. In addition, the codebook design of BS/UE needs improvement as well. I.e. the scenario titled "Utilizing RIS with MIMO: multiplexing and interference management" may not be feasible if the traditional DFT codebook is used. The control of RIS beamforming also needs to be considered. RIS deployment scenarios can have different latency in setting RIS beamforming coefficients, which should be modeled by one suitable parameter in system-level simulations.

8.4.3 Link budget evaluation

The feasibility study of RIS also requires a link budget analysis, which provides the feasible values of RIS sizes, deployment densities, and RIS element gains if necessary. The expected RIS link quality can be derived from such analysis and be used to improve the corresponding PHY and MAC design.

An example of link budget analysis for RIS-aided communication is illustrated in reported in Table 5 shown in the following tables. The tables summarize the main parameters for basic deployment, BS/RIS/UE gain, SINR, and path loss calculation. The analysis calculates the desired Rx power first based on SINR requirements acquired from link-level simulations, and then determines the maximally available path loss considering Tx power and antenna gains. The available path loss is compared to the estimated path loss calculated based on the deployment to check whether the required SINR is achievable.

Table 5: Link budget analysis template for RIS-aided communication

Parameters	Example Values
Basic setup	
Channel for evaluation	PUSCH (/ PDSCH)
Scenario	Urban (/ Office / Special RIS applications)
UE-BS channel model	UMa NLOS O2I
UE-RIS channel model	Indoor Office LOS
RIS-BS channel model	UMa NLOS
Carrier frequency (GHz)	28
BS antenna height (m): depend on Scenario	25
UE antenna height (m): depend on Scenario	1,5
RIS antenna height (m): depend on Scenario	1,5
UE	
(1) Number of UE antenna elements	4
(2) Number of UE chains modeled	1
(3) Total transmit power (dBm)	23
(3a) System bandwidth (Hz) = nRB × nSC(12) × SC_spacing See note 1	72 000 000
(3b) Power spectrum density (dBm/MHz) = (3) - 10log((3a) / 1000000)	4,43
(4) Total UE antenna gain (dB) = (4a) - (4b) + (4c)	6,02
(4a) UE beamforming gain (dB) = 10log((1) / (2))	6,02
(4b) UE antenna gain correction factor (dB)	TBA
(4c) Gain of UE antenna element (dBi)	TBA
(5) Cable, connector, combiner, body, efficiency losses, etc. of UE (dB)	TBA
(6) UE EIRP (dBm) = (3) + (4) - (5)	29,02
RIS	
(7) Number of RIS antenna elements	900
(8) Total RIS antenna gain (dB) = (8a) - (8b) + (8c) See note 2	57,18
(8a) RIS beamforming gain (dB) = 20log((7))	59,08
(8b) RIS antenna gain correction factor (dB)	TBA
(8c) Reflection loss of RIS antenna element (dBi)	-1,9
(9) Cable, connector, combiner, body losses, etc. of RIS (dB)	TBA
BS	
(10) Number of BS antenna elements	256
(10a) Number of BS TxRUs	1
(10b) Number of BS chains modeled	1
(11) Total BS antenna gain (dB) = (11a) - (11b) + (11c)	32,08
(11a) BS beamforming gain (dB) = 10log ((10) / (10a))	24,08
(11b) BS antenna gain correction factor (dB)	TBA
(11c) BS gain of antenna element (dBi)	8
(11bis) Total BS gain of mapping TxRU to RF chains (dB) = (11bis-a) - (11bis-b)	TBA
(11bis-a) BS gain of mapping TxRU to RF chains (dB) = 10log((10a) / (10b))	TBA
(11bis-b) BS gain correction factor for mapping TxRU to RF chains (dB)	TBA
(12) Cable, connector, combiner, body losses, etc. of BS (dB)	TBA
Link budget	
(13) Receiver noise figure (dB)	7

Parameters	Example Values
(14) Thermal noise density (dBm/Hz)	-174
(15) Receiver interference density (dBm/Hz)	-165,7
(16) Total noise plus interference density (dBm/Hz) = 10log(10^(((13) + (14)) / 10) + 10^((15) / 10))	-163,29
(17) Effective noise power (dBm) = (16) + 10log((3a))	-84,72
(18) Required SNR of UE-RIS-BS link (dB)	0,2
(18a) Required SNR of UE-BS link (dB)	-7,1
(19) Receiver implementation margin (dB)	2
(20) HARQ gain (dB) See note 3	TBA
(21) Receiver sensitivity of UE-RIS-BS link (dBm) = (17) + (18) + (19) - (20)	-85,52
(21a) Receiver sensitivity of UE-BS link (dBm) = (17) + (18a) + (19) - (20)	-89,82
(21bis) MCL (dB) of UE-RIS-BS link = (3) - (22) + (11bis), maximum coupling loss	105,52
(21bis-a) MCL of UE-BS link (dB) = (3) - (21a) + (11bis)	112,82
(22) Hardware link budget, also knowns as MIL (dB) = (6) + (8) - (9) + (11) + (11bis) - (12) - (21) See note 4	200,81
(22a) MIL of UE-BS link (dB) = (6) + (11) + (11bis) - (12) - (21a) See note 5	150,92
Available path loss	
(23) Shadow fading margin (dB): function of the cell area reliability and lognormal shadow fading std derivation	5
(24) BS selection/macro-diversity gain (dB)	TBA
(25) Penetration margin (dB) of UE-RIS-BS link: depending on O2O, O2I, high, low, urban, rural, etc.	0
(25a) Penetration margin of UE-BS link (dB): depending on O2O, O2I, high, low, urban, rural, etc.	22,8
(26) Blockage margin of UE-RIS-BS link (dB)	TBA
(26a) Blockage margin of UE-BS link (dB)	TBA
(27) Other gains (dB)	TBA
(28) Other losses (dB)	TBA
(29) UE local geometry loss (dB): the loss caused by UE's orientation, location, etc.	TBA
(30) Available path loss (dB) = (22) - (23) + (24) - (25) - (26) + (27) - (28) - (29)	195,81
(30a) Available path loss of UE-BS link (dB) = (22a) - (23) + (24) - (25a) - (26a) + (27) - (28) - (29)	123,12
Path loss gap	
UE-BS 2D distance (m)	110
RIS-BS 2D distance (m)	105
UE-RIS 2D distance (m)	5
UE-BS 3D distance (m)	112,48
RIS-BS 3D distance (m)	107,60
UE-RIS 3D distance (m)	5
(31) RIS-BS MPL determined by deployment (dB) See note 6	121,89
(32) UE-RIS MPL determined by deployment (dB) See note 7	73,44
(33) Target UE-RIS-BS MPL determined by deployment (dB) (31+32) See note 8 The BS-RIS-UE path loss should be computed as the sum path losses of BS-RIS and RIS-UE, and **not** the path loss of the sum distances of BS-RIS-UE (which only applies to near-field models)	195,32
(33a) UE-BS MPL determined by deployment (dB) See note 6	122,64
GAP of UE-RIS-BS link (dB) = (33) - (30) If positive, then the coverage requirement is NOT achieved	-0,48

Parameters	Example Values
(34a) GAP of UE-BS link (dB) = (33a) - (30a) If positive, then the coverage requirement is NOT achieved	-0,48
NOTE 1: SC_spacing = 120 kHz, nRB = 50. NOTE 2: RIS gain is also limited by the pathloss. NOTE 3: Only applicable if HARQ is not considered in simulator. NOTE 4: MIL can also be derived by (21bis) + (4) - (5) + (8) - (9) + (11) - (12), maximum isotropic loss. NOTE 5: MIL can also be derived by (21bis-a) + (4) - (5) + (11) - (12). NOTE 6: Here the MPL is calculated based on UMa NLOS model in ETSI TR 138 901 [i.2]. NOTE 7: Here the MPL is calculated based on Indoor Office LOS model in ETSI TR 138 901 [i.2]. NOTE 8: Determined by scenario, distance, height, and carrier frequency.	

An example setup for a simple UL analysis is provided based on ETSI TR 137 910 [i.20] while the path loss and channel models are defined based on the ETSI TR 138 901 [i.2]. The link-level simulation parameters are used to get the required SNR in **(18)** and **(18a)** (see the tables) are given in Table 6.

**Table 6: Link-level simulation parameters used to get
the required SNR for RIS-aided link budget analysis**

LLS parameters for PUSCH simulations	Values / setups	Comment
Carrier frequency	28 GHz	
Subcarrier spacing	120 kHz	
Number of RBs	50	
Bandwidth	72 MHz	
Waveform	DFT-S-OFDM	
UL / DL	UL	UL ratio is set to 30 %
LLS fading channel models	CDL-A / CDL-E / LOS	Scenario-dependent
Number of Tx chains at UE	1	
Number of Rx chains at BS	1	
Duration of PUSCH	14 OFDM symbols	
DMRS	Type A and type 1, 1 OFDM symbol	
MCS	3	
Channel estimation	Practical	
Synchronization	Practical	
UL Throughput requirement	5 Mbps	SNR requirements are acquired based on LLS results

The generated throughput-SNR curves using different fading channel models are plotted in Figure 35.
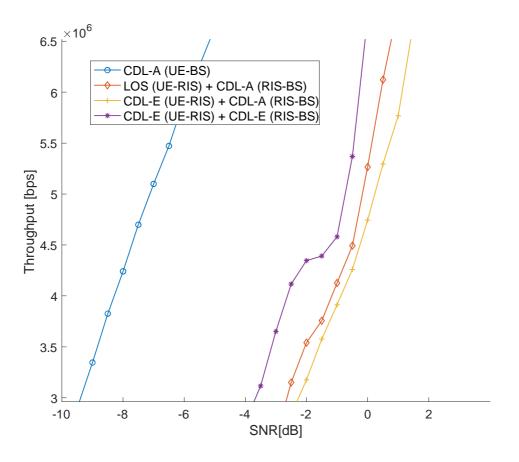
Figure 35: Throughput-SNR curves of different channel models generated by LLS

Next, link budget analysis is performed on a few typical RIS scenarios. Specifically, the number of RIS elements that allows comparable UL throughput performance to UE-BS direct link and achieves the required UL throughput is explored in the proposed scenarios.

In the first proposed scenario, shown in Figure 36, and RIS is used to avoid penetration losses between the UE and BS.
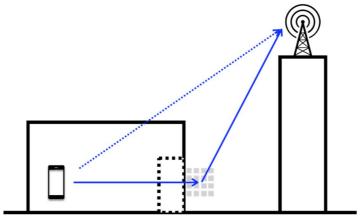

Figure 36: Scenario I - Using RIS to avoid penetration loss

The link budget analysis assumptions and results are listed in Table 7, in which 900 RIS elements are enough to achieve the required UL throughput.

Table 7: Link budget analysis assumptions and results corresponding to Scenario I

Link	UE-BS	UE-RIS-BS
Number of RIS elements	N/A	900 (16,1 cm x 16,1 cm)
Channel model	UMa NLOS O2I	InH LOS + UMa NLOS
LLS channel model	CDL-A with 300 ns delay spread, doppler shift 77,78 Hz (i.e. UE speed is 3 km/h)	UE-RIS: CDL-E with 30 ns delay spread, doppler shift 77,78 Hz RIS-BS: CDL-A with 300 ns delay spread
O2I loss (dB)	22,8	0
2-D distance (m)	110	UE-RIS: 5 RIS-BS: 105
Path loss (dB)	145,44	195,32
Rx SNR (dB)	-6,62	0,68
SNR required (dB)	-7,1	0,2
Excess SNR (dB)	0,48	0,48

In the second proposed scenario, shown in Figure 37, a UE-controlled RIS is used to provide diversity gain against UE's rotation and self-blockage.
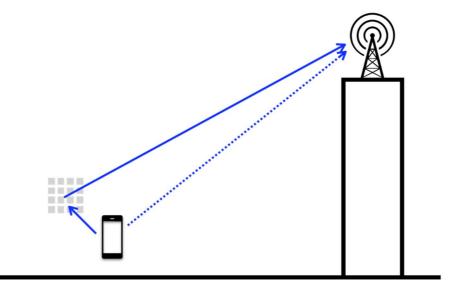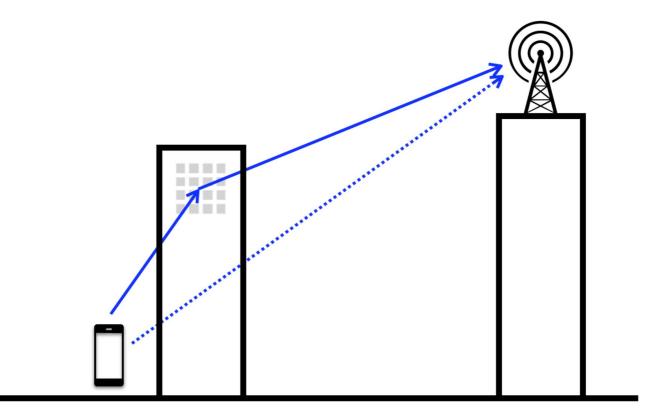

Figure 37: Scenario II - UE-controlled RIS to provide diversity gain against UE's rotation and self-blockage

The link budget analysis assumptions and results are listed in Table 8, in which 6 400 RIS elements are enough to achieve the required UL throughput.

Table 8: Link budget analysis assumptions and results corresponding to Scenario II

Link	UE-BS	UE-RIS-BS
Number of RIS elements	N/A	6 400 (42,9 cm x 42,9 cm)
Channel model	UMa NLOS	InH LOS + UMa NLOS
LLS channel model	CDL-A with 300 ns delay spread, doppler shift 77,78 Hz (i.e. UE speed is 3 km/h)	UE-RIS: LOS, doppler shift 77,78 Hz RIS-BS: CDL-A with 300 ns delay spread
O2I loss (dB)	0	0
2-D distance (m)	440	UE-RIS: 2 RIS-BS: 440
Path loss (dB)	145,81	213,18
Rx SNR (dB)	-6,99	-0,13
SNR required (dB)	-7,1	-0,2
Excess SNR (dB)	0,11	0,07

The third proposed scenario, shown in Figure 38, depicts the street canyon application of RIS.

Figure 38: Scenario III - RIS serves UE in a street canyon

The link budget analysis assumptions and results are listed in Table 9, in which 4 096 RIS elements are enough to achieve the required UL throughput.

Table 9: Link budget analysis assumptions and results corresponding to Scenario III

Link	UE-BS	UE-RIS-BS
Number of RIS elements	N/A	4 096 (34,3 cm x 34,3 cm)
Channel model	UMa NLOS	UMi LOS + UMa LOS
LLS channel model	CDL-A with 300 ns delay spread, doppler shift 77,78 Hz (i.e. UE speed is 3 km/h)	UE-RIS: CDL-E with 30 ns delay spread, doppler shift 77,78 Hz RIS-BS: CDL-E with 30 ns delay spread
O2I loss (dB)	0	0
2-D distance (m)	440	UE-RIS: 40 RIS-BS: 400
Path loss (dB)	145,81	209,38
Rx SNR (dB)	-6,99	-0,21
SNR required (dB)	-7,1	-0,8
Excess SNR (dB)	0,11	0,59

The fourth proposed scenario, shown in Figure 39, quantitatively evaluates the capability of RIS to extend the cell coverage.
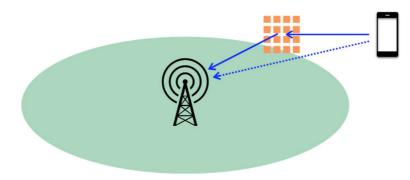

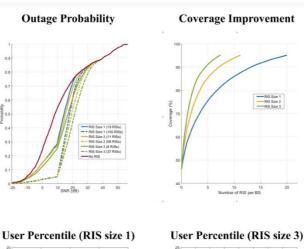**Figure 39: Scenario IV - RIS extends the network coverage**

The link budget analysis assumptions and results are listed in Table 10. Without RIS, the cell coverage is 110 m. The cell coverage can reach about 170 in aided by RIS with at most 129 600 elements.
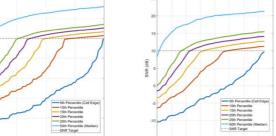
Table 10: Link budget analysis assumptions and results corresponding to Scenario IV

Link	UE-BS	UE-RIS-BS		
Number of RIS elements	N/A	44 100 (1,13 m x 1,13 m)	90 000 (1,61 m x 1,61 m)	129 600 (1,93 m x 1,93 m)
Channel model	UMa NLOS O2I	UMi LOS + UMa NLOS (assume the same O2I loss)		
LLS channel model	CDL-A with 300 ns delay spread, doppler shift 77,78 Hz (i.e. UE speed is 3 km/h)	UE-RIS: CDL-E with 30 ns delay spread, doppler shift 77,78 Hz RIS-BS: CDL-A with 300 ns delay spread		
O2I loss (dB)	22,8	22,8	22,8	22,8
2-D distance (m)	110	UE-RIS: 20 RIS-BS: 110	UE-RIS: 40 RIS-BS: 110	UE-RIS: 60 RIS-BS: 110
Path loss (dB)	145,44	229,54	235,30	238,89
Rx SNR (dB)	-6,62	0,27	0,70	0,28
SNR required (dB)	-7,1	0,2	0,2	0,2
Excess SNR (dB)	0,48	0,07	0,50	0,08

Finally, a system-level simulation study for RIS-aided system is reported in [i.18]. Specifically, the benefits of adding RIS have been evaluated in terms of coverage probability and per resource block rate for different user percentiles, which include the typical UEs (the 50th percentile of UEs) and the cell-edge UEs (the 5th percentile of UEs), by assuming that a UE is in coverage if the received SNR is greater than 10 dB in order to create coverage-boosted areas. Overall, the system-level simulations reveal that the deployment of RIS enhances the coverage probability of the UEs from 77 % to 95 % in the C-band and from 46 % to 95 % in the mmWave band. The deployment of only 5 RIS per BS whose size is 3,8 m × 3,8 m in the C-band and 0,67 m × 0,67 m in the mmWave band ensures that 90 % of the UEs are in coverage. If 12 RIS per BS of the same size are deployed, the per resource block rate of the cell-edge UEs increases by a factor of 3,5 and by a factor of 25 in the C-band and mmWave band, respectively. In the mmWave band, the SNR of the cell-edge UEs increases by 20 dB if, for each BS, 20 RIS whose size is 0,33 m × 0,33 m or 8 RIS whose size is 0,67 m × 0,67 m are deployed. In the presence of network interference, in addition, the SINR coverage probability increases from 46 % to 92 % if, for each BS, 8 RIS whose size is 0,67 m × 0,67 m are deployed.

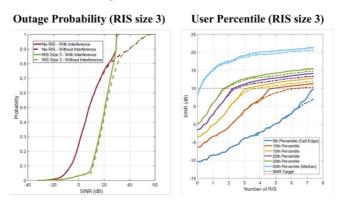Illustrative results are reported in Figure 40 for application to the mmWave frequency band.

Figure 40: Application to the mmWave frequency band

Millimeter-wave (28 GHz) system-level analysis as a function of the size of the RIS. Size 1: 0,33 m × 0,33 m; size 3: 0,67 m × 0,67 m (top) SNR coverage of the UEs when the target SNR threshold is set to 10 dB. (center) Received SNR of different percentiles of UEs as a function of the size of the RIS. (bottom - impact of interference) SINR coverage of the UEs when the target SINR threshold is set to 10 dB and 37 RIS are deployed (left figure); and received SINR for different percentiles of UEs (right figure).

9   Conclusions

The present document summarizes ETSI ISG RIS views on communication models, channel modeling, channel estimation methods, and evaluation methodology for RIS-integrated communications, localization, and sensing use cases. The findings can serve as a reference point for relevant specifications and standards to model and evaluate RIS-integrated systems.

History

Document history		
V1.1.1	June 2023	Publication